



# Multi-scale characterization from the Hard Cap, Mupe Member, Lower Purbeck Limestone Group, Wessex Basin, Dorset, UK

Rafael Cremonini Baptista<sup>1</sup> · Sérgio Bergamaschi<sup>1</sup> · Marcus Vinicius Berao Ade<sup>1</sup> · Alessandra Silveira Machado<sup>2</sup> · Olga Maria Oliveira de Araújo<sup>2</sup> · Ricardo Tadeu Lopes<sup>2</sup> · Giovanni C. Stael<sup>3</sup>

Received: 28 February 2023 / Revised: 3 May 2023 / Accepted: 9 May 2023 / Published online: 21 May 2023  
© The Author(s), under exclusive licence to Springer Nature Switzerland AG 2023

## Abstract

Non-marine carbonates are not fully understood from several points of view, including facies and petrophysics (porosity and permeability), as well as their controlling processes. The Hard Cap of the Mupe Member in the Purbeck Limestone Group of the Wessex Basin contains thrombolites presenting varying porosity degrees. This paper aims to carry out a multi-scale characterization, focusing on Mupe Member petrophysical properties and providing insights into its depositional environments and diagenetic history. Non-marine carbonates are characteristically heterogeneous, and their components are highly diverse, comprising various types of primary micrites, bioclasts and other particles, as well as different types of cement precipitated at different diagenetic stages. These components display distinct geochemistry and petrophysics signatures. This study integrates microtomography, petrographic, geochemistry, and petrophysics data from Hard Cap Purbeck samples obtained from a block store at the Bowers Quarry in Portland (50°32′49.4″ N, 2°26′53.1″ W), with the aim of better understanding these challenging reservoirs. Hard Cap porosity is predominantly the result of bioturbation and dissolution. Organisms such as ostracods and gastropods are believed to have played a key role in porosity development, as their activity resulted in sediment mixing and the development of pore spaces. Carbonate mineral dissolution also contributed to porosity development, with the most significant dissolution occurring during periods of increased groundwater flow. A stable isotope analysis indicated that dissolution was likely the result of acidic groundwater, which can dissolve carbonate minerals present in the limestone. The Hard Cap cementation process is the primary cause of its low porosity and permeability. The analysis also revealed that the Hard Cap was deposited in a shallow environment with alternating subaerial exposure and inundation periods. The paleo controls concerning Hard Cap porosity development were found to be largely associated to lake level and climate changes. During high lake level periods, the Hard Cap was submerged and subject to increased sedimentation, reducing porosity development. Conversely, during low lake level periods, the Hard Cap was exposed to increased groundwater flow, promoting dissolution and porosity development. Overall, this study provides important insights into the porosity origin of the Mupe Member Hard Cap and the paleo controls that influenced its development. These findings may be useful in the exploration and development of hydrocarbon reservoirs located in similar geological settings.

**Keywords** Microbialites · Purbeck · X-ray microtomography · Geochemistry · Petrographic · Petrophysics

---

Communicated by M. V. Alves Martins

✉ Rafael Cremonini Baptista  
rafael.baptista@uerj.br

<sup>1</sup> Faculdade de Geologia Departamento de Estratigrafia e Paleontologia, Universidade do Estado do Rio de Janeiro, UERJ, Rio de Janeiro, Brazil

<sup>2</sup> Universidade Federal do Rio de Janeiro, UFRJ/COPPE/Programa de Engenharia Nuclear, Rio de Janeiro, Brazil

<sup>3</sup> Observatório Nacional (National Observatory), Rio de Janeiro, Brazil

## 1 Introduction

Non-marine carbonates are a diverse group of sedimentary rocks formed in various environments, including lakes, rivers, caves, and soils. Despite their abundance and importance, non-marine carbonates have received relatively little attention compared to their marine counterparts (Capezzuoli et al., 2022). The discovery of the prolific ultra-deep pre-salt field in Brazil, along with significant discoveries in China, has led to significant scientific interest in carbonate rocks located in non-marine rift environments.

Interpreting the occurrence, formation, and significance of non-marine carbonates is essential for a comprehensive understanding of carbonate reservoirs. Carbonate sediments are prone to rapid and pervasive diagenetic alterations that modify carbonate rock mineralogy and pore structure cementation and dissolution processes, in particular, continuously modifying pore structures to create or destroy porosity (Eberli et al., 2003).

A literature review revealed that non-marine carbonates are a diverse group of sedimentary rocks formed in various environments, including lakes, rivers, caves, and soils (Capezzuoli & Swennen, 2017; Capezzuoli et al., 2022). The most common types of non-marine carbonates are travertine, tufa, calcareous soils, and calcretes (Jones & Renaut, 1995). The formation of non-marine carbonates is mainly controlled by complex chemical and biological processes, including precipitation, dissolution, and microbial activity (Capezzuoli & Swennen, 2017).

The complex, heterogeneous, and deformed pore structures of the aforementioned pre-salt field in Brazil make petrophysical characterizations and formation process evaluations a challenge for the Oil Industry (Ahr, 2008). Brazilian Pre-salt carbonates are not fully understood from several perspectives, including petrophysics, facies, diagenesis, and structural geology. Additionally, access to Brazilian pre-salt carbonate rocks is difficult. On account of this, analog rocks are essential to understand the growth, facies and petrophysical properties of these carbonates.

The Purbeck Limestone Group (Upper Jurassic–Lower Cretaceous) exposed in Dorset is considered a partial analogue regarding some South Atlantic pre-salt carbonate reservoir aspects, as both deposits are about the same age, presenting similar tectonic setting and basin evolution (both are pre-salt carbonates) and porous microbial mound facies (Gallois & Bosence, 2017). Lower Purbeck Formation carbonates comprise microbialites (thrombolites and stromatolites) with unusual growth patterns (Muniz & Bosence, 2015). Overall, the Lower Purbeck Limestone is a useful partial analogue for some aspects of the Brazilian pre-salt carbonate reservoirs due to their similarities in age, tectonic setting, and basin evolution. Based on the search results provided by Gallois & Bosence, 2017 the potential points to consider when using the lower Purbeck Limestone as a partial analogue of Pre-salt carbonate from the South Atlantic:

- (1) Depositional environment: The lower Purbeck Limestone was deposited in a shallow non-marine environment that was low-energy and protected from wave action. Similarly, the pré-sal carbonate reservoirs were deposited in a shallow non-marine environment that was relatively calm and protected from the open ocean.
- (2) Lithology: The lower Purbeck Limestone is a carbonate rock that contains a variety of facies, including mud-

stones, wackestones, packstones, and grainstones. Similarly, the pré-sal carbonate reservoirs are composed of different carbonate facies, including limestones, dolomites, and anhydrites.

- (3) Organic matter: The lower Purbeck Limestone contains organic matter, which can provide insights into the thermal maturation and diagenesis of the rocks. Similarly, the Pre-salt carbonate reservoirs also contain organic matter, which can affect the porosity and permeability of the rocks.
- (4) Diagenesis: The lower Purbeck Limestone has undergone extensive diagenesis, including compaction and cementation. Similarly, the Pre-salt carbonate reservoirs have undergone significant diagenesis, including cementation, and fracturing.
- (5) Reservoir properties: The lower Purbeck Limestone has different range of permeability and porosity, which can make it a useful analogue for the Pre-salt carbonate reservoirs, which also have variable permeability and porosity.

By considering these and other factors, researchers can use the lower Purbeck Limestone as an analogue for the Pre-salt carbonate reservoirs, providing valuable insights into the depositional environment, lithology, diagenesis, and reservoir properties of these important geological formations. Because of this, the Purbeck Formation offers an excellent opportunity to further knowledge on petrophysical responses and their association with different facies to more accurately evaluate and characterize microbial carbonates by employing non-destructive X-ray microtomography (microCT) analyses for digital rock assessments.

Purbeck microbialites are exposed on the Isle of Portland, Dorset, in southern England (Fig. 1). They display characteristic freshwater tufa features (Bosence, 1987; Perry, 1994), presenting mainly thrombolitic textures. The Mupe Member of the Purbeck Limestone Group is particularly well exposed in its type area along the south Dorset coast, comprising part of the Jurassic Coast World Heritage Site (Gallois, 2016).

Thrombolites are sedimentary structures composed of microbial communities that form thin, laminated layers. They are most commonly found in shallow, freshwater environments and are formed by the accretion of microbial communities onto existing sediment structures. The microbial communities that form thrombolites are usually composed of bacteria, archaea, and cyanobacteria. Thrombolites are usually characterized by dome- or column-shaped structures composed of thin layers of sediment interbedded with microbial remains (Kennard & James, 1986). Thrombolite formation is a complex process that involves a combination of biological, chemical, and physical processes (Reid, 2001).

Understanding the formation and composition of thrombolites can provide insights into the evolution of this

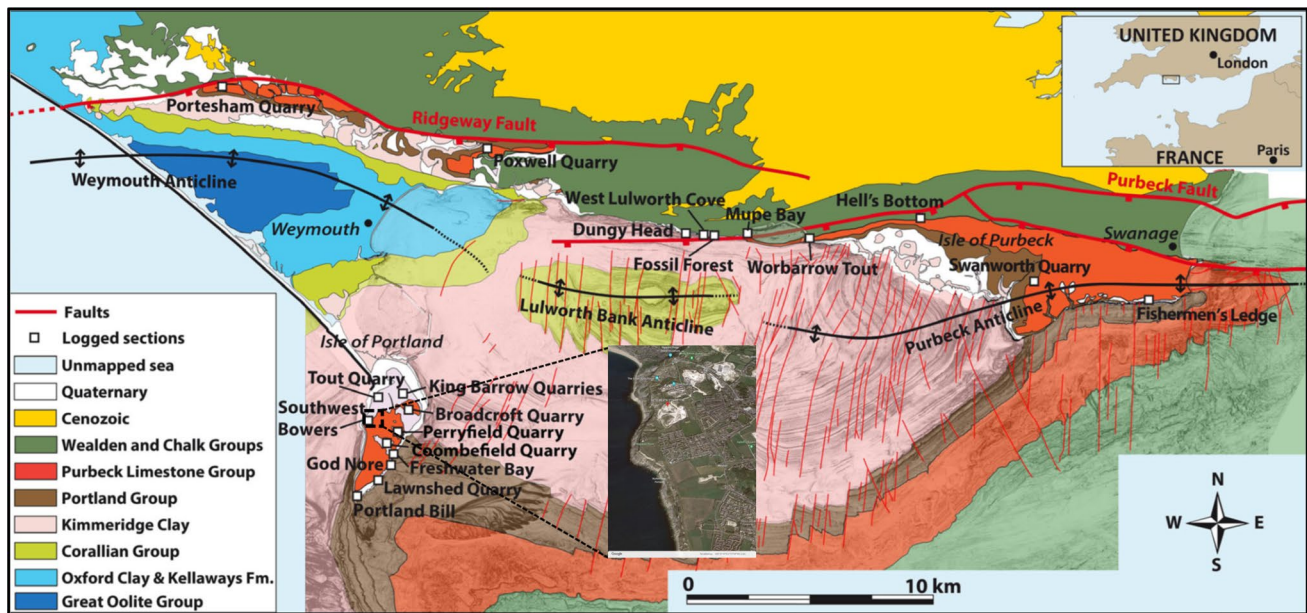


**Fig. 1** Location and geological maps of the study area. The block comes from the Hard Cap unit and was obtained from a store of similar blocks at Bowers Quarry in Portland.  $50^{\circ}32'49.4''$  N  $2^{\circ}26'53.1''$  W. Modified from Bosence and Gallois (2022)

challenging reservoir. Recent studies have applied multi-scale characterizations to better understand thrombolites. For example, the studies conducted by Boomer et al. (2003) and Liu et al. (2017) employed multi-scale characterization, a powerful tool for investigating the complex structure and composition of geological materials. This technique involves applying various analytical techniques to investigate materials at different scales.

Outcrop studies of the Upper Jurassic-Lower Cretaceous (Tithonian) Lower Purbeck Limestone Group strata along the southern coast of England in the Isle of Portland/Lulworth/Worbarrow Bay area (Fig. 1) have revealed a distinctive succession of limestones, calcareous shales, and marls. These strata are up to 120 m thick onshore (Clements, 1993; West, 1975) and over 200 m thick offshore (Underhill, 2002), and contain diverse fossil assemblages that sometimes indicate fresh, often brackish or hypersaline, and occasionally, fully marine deposition conditions (Batten, 2002; Coram & Radley, 2021).

This study aims to carry out a multi-scale analysis of the Hard Cap in the Mupe Member, with the following objectives:

- (1) Characterize Hard Cap mineralogy and texture using thin-section petrography.
- (2) Determine Hard Cap porosity and permeability using porosity and permeability laboratory measurements.
- (3) Evaluate the impact of mineralogy and texture on Hard Cap petrophysical properties, including the interpretation and analysis of the gamma-ray logs to determine

the depositional environment of the limestone samples and their Th/U ratios.

- (4) Characterize the internal structure and morphology of thrombolites using high-resolution X-ray microtomography and evaluate the potential of X-ray microtomography as a tool for thrombolite characterization.
- (5) Analyze stable carbon and oxygen isotopes to determine the depositional environment and diagenetic alteration histories of limestone samples.

The results of this study will provide a better understanding of the geological history and petrophysical properties of Mupe Member Hard Caps, as the applied methodologies can be used to improve reservoir characterization and hydrocarbon exploration in similar geological settings.

## 2 Geologic setting

### 2.1 The Wessex Basin

The Wessex Basin was formed during the Late Permian and evolved during subsequent extensional and compressional tectonic events that took place in the Mesozoic and Tertiary (Butler, 1998; Hawkes et al., 1998; Underhill & Stoneley, 1998). It is an established hydrocarbon province (Underhill & Stoneley, 1998) and several studies have described the geological evolution of both the Wessex Basin and Purbeck Group for over 200 years (Anderson & Bazley, 1971; Anderson 1973; Bosence & Gallois, 2022; Francis, 1982, 1984;

Gallois, 2016; Horne et al., 2002; Perry, 1994; Pugh, 1968; Underhill, 2002; Underhill & Stoneley, 1998; Webster, 1826; West, 1975; Woodward, 1895).

The Wessex Basin is an extended sub-basin within a larger intracratonic system of Mesozoic basins covering much of north-western Europe (Underhill & Stoneley, 1998; Ziegler, 1990), which was transformed by north–south compression during the Cenozoic. The initial extent of the Wessex Basin was compiled from outcrop and subsurface data (Cope 1980; Lake, 1985; Underhill, 2002), indicating occasional oceanic connections to the southwest and north-east (Cope et al., 1999). The Wessex Basin comprises three sub-basins, namely the Portland-Wight in the southwest, the Pewsey in the northwest and the Weald in the east.

Wessex Basin sediments are recorded in sandstones, shales, limestones and evaporites from the Permian to the Cenozoic, with subsequent post-Cenozoic deposits noted in the Hampshire Basin (Fig. 2; Gallois, 2016 modified after Underhill & Stoneley, 1998).

## 2.2 Mupe Member–Lower Purbeck Limestone Group

The Purbeck Limestone Formation includes non-marine carbonate, evaporite, and paleosol facies from the Upper Jurassic to the Lower Cretaceous (Bosence, 1987; Perry, 1994; West, 1975). The Mupe Members of the Purbeck Limestone Formation, a part of the Jurassic Coast World Heritage Site and the subject of this study, are particularly well exposed in the type area on the southern coast of Dorset (Fig. 1). Non-marine sediments of Mupe Members (Fig. 2b) have been periodically studied for almost 200 years, with most publications focusing on the middle and upper parts of the group, well exposed in Durlston Bay (Clements, 1993; Wimbledon & Hunt, 1983).

Less research, however, has been performed on the lower details of Mupe Members (Westhead & Mather, 1996), including “caps” and “mud beds” by earlier authors, as well as “broken beds” and “Cypris Freestones” (Clements, 1993).

Mupe Members are composed of Upper Jurassic lacustrine microbial carbonates, and their associated facies were formed in a semi-arid climate setting during the extensional phase of Wessex Basin (Gallois & Bosence, 2017), occurring within three stratigraphic horizons, termed Skull Cap, Hard Cap, and Soft Cap (Fig. 3), separated by palaeosol horizons known as ‘dirt beds’ (Gallois et al., 2018; Perry, 1994; West, 1975, 2013).

According to Gallois (2016), these represent three shallowing-upward lacustrine sequences capped by emergent surfaces (paleosols). Thrombolites typically grow as mounds up to 10 m across and vary in thickness from about 0.5–4 m, maintaining a high primary framework porosity (Gallois & Bosence, 2017). These structures commonly accumulated

around the bases of contemporaneous trees or fallen tree trunks (now silicified or represented by moulds) initially on a burrowed boundstone substrate (Gallois et al., 2018) (Fig. 4). Vugs are abundant and conspicuous calcite crusts with smooth botryoidal upper surfaces that commonly surround mesoclots or cap thrombolites (Kirkham & Tucker, 2018).

## 3 Materials and methods

This study is based on a detailed analysis of a 4.5-ton block (Fig. 5) from the Hard Cap unit obtained from a store of similar blocks at Bowers Quarry in Portland (50°32′49.4″ N 2°26′53.1″ W). The block was donated by Baker Hughes of Brazil to the Rio de Janeiro State University (Universidade do Estado do Rio de Janeiro, UERJ). A total of 29 core samples (1.0 inches in diameter) were taken and faceted. From these, a set of 17 plugs from bottom to top parallel to the sedimentary bedding were used in microtomography, petrophysics, geochemistry, and petrographic analyses.

The core samples were imaged using a microCT in a Phoenix Vltomelx M equipment (Waygate Technologies) at the Nuclear Instrumentation Laboratory belonging to the Federal University of Rio de Janeiro (COPPE Nuclear Engineering Program, UFRJ). The images were obtained at a 25 µm effective pixel size resolution, and the scanning parameters were set to 100 kV and 250 µA operating voltage and current, with a 250 ms exposure time. An aluminum filter (1 mm) was used to improve image quality. Porosity measurements were performed using the CTAn software v. 1.17.7.2 and permeability measurements were conducted using the Avizo Fire software v. 2020.1, employing the Xlab Absolut Permeability Simulation plugin.

The plugs underwent routine petrophysical characterizations to obtain effective porosity and absolute permeability values using a UltraPore 300 and UltraPerm 500 (Core Lab) gas porosimeter and permeameter, respectively at the National Observatory Petrophysics Laboratory (Lab-PetrON). A matrix cup and plug core-holder with a standard diameter of 1.0 and 1.5 inches and variable lengths up to 10.0 cm, were used. Nitrogen was used for porosity and permeability measures at a pressure of 500 psi.

The gamma-ray spectrometry data were obtained using a portable GRS-2000 detector gamma-ray spectrometer at the Chemostratigraphy and Organic Geochemistry Laboratory (LGQM-UERJ). The GRS-2000 instrument was calibrated using high volume standards (etalons) for K, Th and U at the Brazilian Nuclear Energy Commission Institute of Radiation Protection and Dosimetry (IRD) under the authority of the Brazilian Ministry of Science, Technology, and Innovation. The GRS data acquisition procedure consisted in two measures. The first measurement was obtained by maintaining the

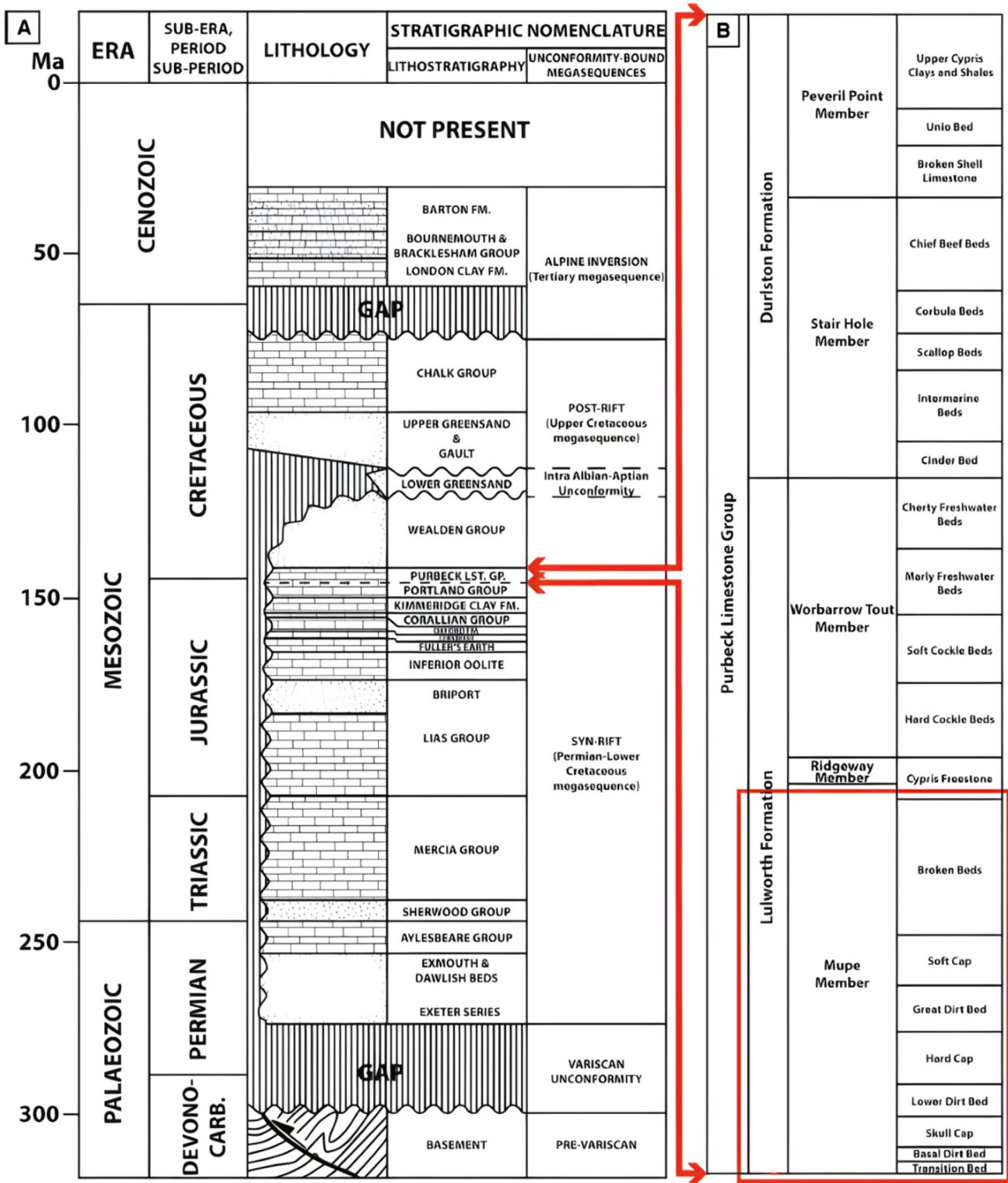


Fig. 2 Wessex Basin stratigraphic divisions: **A** Wessex Basin stratigraphy (Gallois, 2016, modified after Underhill & Stoneley, 1998); **B** detailed Purbeck Limestone Group stratigraphy

detector in contact with the plug position on the block for 120 s, and the second measurement was obtained by repeating the same procedure. The final value consisted of the

average of the two measures for the determined K (%), Th (mg/kg) and U (mg/kg) peaks.



**Fig. 3** Lower part of the Mupe Member Outcrop – God Nore, Isle of Portland. Photograph taken by R. C. Baptista

Stable  $\delta^{13}\text{C}$  (‰) VPDB and  $\delta^{18}\text{O}$  (‰) VPDB Isotopes were determined employing an advanced spectrometer isotope ratio mass (IRMS) Kiel IV Carbonate equipment connected to a Thermo Delta V Advantage equipment at the LGQM. Sample processing was performed according to McCrea (1950). The carbon and oxygen stable isotope analyses were performed in  $\sim 3$  g of a total rock sample from each core, focusing on comparative analyses. The 17 samples were sorted, homogenized by maceration, and sieved through an 80-mesh grain size and then reacted with 103% phosphoric acid at 25 °C according to McCrea (1950). Analytical accuracy and replicate analyses were always better than 0.1‰.

The metrographic microscopy analyses were performed using a Zeiss Axio Lab A1 petrographic microscope at the Petrography Laboratory (LPETRO) belonging to the Geology Faculty of UERJ. A set of 17 thin sections (one of each core sample) was described petrographically and sedimentological, using the Dunham (1962) carbonate rock classification. Thin section analyses allowed for more detailed assessments of the mineralogical composition, fossil record, and pore types of the studied carbonate rocks.

## 4 Results and discussion

Porosity and permeability are key factors in oil and gas exploration, and understanding their origin is crucial to identify areas that may be conducive to hydrocarbon production.

An integrated analysis is presented herein to understand the physical changes of the studied Hard Cap thrombolite. A comprehensive study was conducted to understand permeability and porosity variations across the Hard Cap samples.

### 4.1 Gamma-ray spectrometry

The gamma-ray logs indicated significant variations in the total units of the limestone samples from the Hard Cap. High total values indicate the Mudstone-Wackestone facies, while the low total gamma ray values indicate microbialite (thrombolite) layers. Variations in total gamma-ray values also suggest changes in the depositional environment and diagenetic alteration history of the limestone samples.

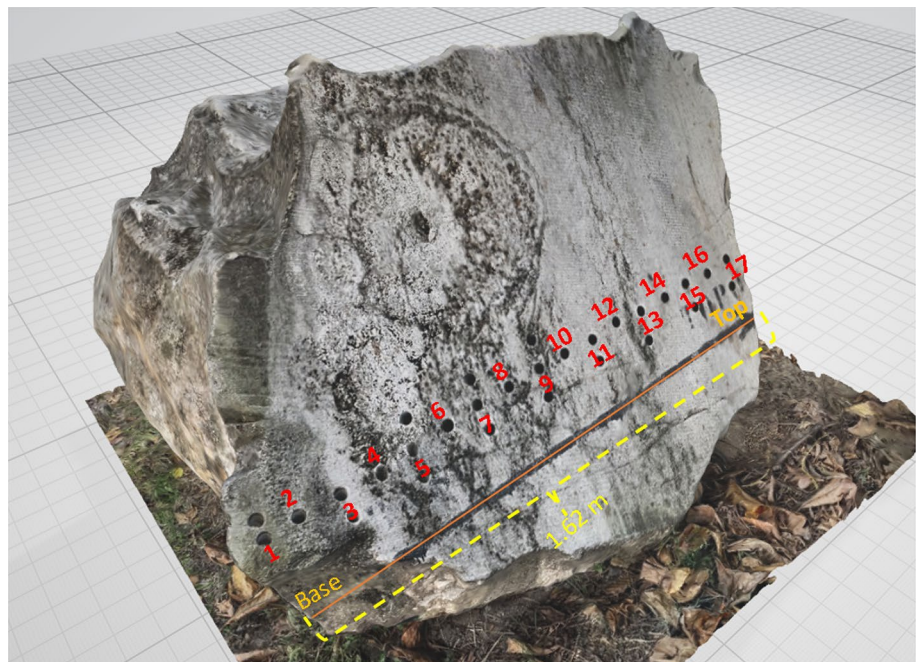
The Th/U ratios were determined by analyzing the gamma-ray spectra of the samples obtained from the Hard Cap, Mupe Member using a gamma ray log.



**Fig. 4** Left—A mould of a fallen branch initially surrounded by burrowed boundstone (smooth) and later by thrombolites (rubbly). Field notebook for scale. Right—Centimeter-sized microbial intraclasts adja-

cent to a microbial mound, originally developed around a tree trunk that has since been removed by erosion, leaving a hollow mound center. Field notebook for scale. R. C. Baptista took the photograph

**Fig. 5** The 4.5-ton block from the Hard Cap unit obtained from a store of similar blocks at Bowers Quarry in Portland (50°32'49.4" N 2°26'53.1" W). The numbers of the analyzed plugs are depicted in red



The Th/U ratios varied, ranging from 3.7 to 6.8, indicating significant differences in the physical changes that occurred in the Hard Cap layers. The low Th/U ratio suggested that the limestone layers underwent minimal physical

changes during burial, while the high Th/U ratio suggested greater physical changes.

The gamma-ray spectrometry results are presented in Table 1.

**Table 1** Gamma-ray spectrometry results

Plug	TOT	Dose Rate	K (cps)	K (%)	U (cps)	U (mg/kg)	Th (cps)	Th (mg/kg)	CC (cps)	DT (%)	Th/U
1	1443.39	48.3	5.735	1.65	2.4	2.05	1.79	13.7	0.83	2.4	6.683
2	1440.78	43.25	5.205	1.35	2.39	2.1	1.67	12.5	0.825	2.3	5.952
3	1438.87	39.55	4.29	1.05	2.115	2.35	1.415	9.25	0.91	2.3	3.936
4	1.432.775	27.85	3.97	1	2.075	2.05	1.285	8.65	0.78	2.3	4.220
5	1.423.675	10.35	3.63	0.9	1.635	1.3	1.12	7.05	0.785	2.3	5.423
6	1.427.265	17.25	3.425	0.85	1.605	1.1	1.2	7.5	0.78	2.3	6.818
7	1.423.955	10.9	3.73	0.95	1.675	1.5	1.23	7.2	0.74	2.3	4.800
8	1.431.745	25.85	3.685	0.9	1.655	1.25	1.24	7.3	0.785	2.3	5.840
9	1428.21	19.1	3.41	0.8	1.73	1.5	1.075	6.35	0.815	2.3	4.233
10	1.427.435	17.6	3.515	0.85	1.75	1.15	1.2	7.5	0.82	2.3	6.522
11	1.430.695	23.8	3.395	0.85	1.84	1.5	1.14	6.8	0.84	2.3	4.533
12	1.430.775	24	3.37	0.75	1.885	1.85	1.155	7.05	0.815	2.3	3.811
13	1.427.685	18.05	3.425	0.8	1.835	1.4	1.195	7.65	0.88	2.3	5.464
14	1428.5	19.65	3.435	0.8	1.79	1.8	1.14	6.7	0.855	2.3	3.722
15	1426.55	15.85	3.815	0.95	1.895	1.75	1.255	8	0.825	2.3	4.571
16	1.432.955	28.2	3.77	0.9	1.94	1.95	1.285	8.15	0.93	2.3	4.179
17	1438.31	38.5	4.57	1.2	2.255	2.2	1.675	11.5	0.895	2.3	5.227

The TOT symbol represents the total spectrum count and dose rate value in nGy/h. The K symbol represents the potassium (K) count and the K concentration in %. The U symbol represents the uranium (U) count and the U concentration in mg/kg. The Th symbol represents the thorium (Th) count and the Th concentration in mg/kg. The CC symbol represents the cosmic count. The DT symbol represents the dead time percentage

The natural gamma radiation of rocks is the result of emissions produced by potassium (K), thorium (Th), and uranium (U) isotopes (Dypvik & Eriksenf, 1983; Ehrenberg & Svånå, 2001). The relative contributions of these elements to the total gamma ray (GR) log profile of a borehole can be differentiated by a spectral GR logging tool, and such patterns are commonly examined in hydrocarbon exploration wells as a means of estimating mineralogy, differentiating depositional environments, and recognizing significant stratigraphic surfaces (Davies & Elliott, 1996; North & Boering, 1999; Serra, 1984). Scarce studies documenting spectral GR significance are available to date for carbonate strata, although there appears to be a widespread appreciation that K and Th reflect clastic content, whereas U is determined by diagenetic processes involving oxidation state changes (Lucia, 1999). Most of the published carbonate spectral GR assessments ascribe localized U enrichment to late diagenetic fluid movements (Fertl & Rieke, 1980; Hassan et al., 1976; Luczaj, 1998).

According to Klaja and Dudek (2016), the application of the spectral gamma record in geological interpretation is much better recognized by Th/U ratio curves, where Th/U ratios can reflect sedimentary conditions, as follows: Th/U > 7 indicating continental environment, oxidizing conditions and weathered soils, among others, Th/U < 7, indicating marine sediments, grey and green shales and greywacke and Th/U < 2, marine black shales, phosphorites and reducing conditions. Organic matter content estimates

in the claystone and detection of stratigraphic correlations determine transgressive–regressive and oxidant-reducing conditions.

The gamma-ray spectrometry results suggest that the Hard Cap Mupe Member of the Lower Purbeck Limestone Group is a layered formation consisting of alternating layers of Mudstone-Wackestone, Microbialite, and Peloid grainstone. The detected variations in Th/U ratio values also suggest changes in the depositional environment, including lake level fluctuations and sediment supply changes. The high Th/U ratio values indicate that the limestone layers were deposited in a high-energy shallow environment, whereas the low Th/U ratio values suggest deposition in a low-energy environment with restricted circulation.

## 4.2 Routine petrophysics analyses

The routine petrophysical characterization results obtained at LabPetrON are displayed in Table 2. The grain density values ranged between 2.63 and 2.71 g/cc, consistent with the mineralogical composition determined by petrographic and microCT analyses. The seventeen analyzed plugs displayed variable porosity and permeability values and can be separated into three categories considering permeability values, very low (< 3 mD), low (3–13 mD) and very high (> 1000 mD) permeability. The porosity and permeability of samples 4, 8, 15 and 16 could not be determined due to diameter changes along the plugs.



**Table 2** Purbeck plugs routine petrophysical data

Plug	Density (g/cm <sup>3</sup> )	Porosity (%)	Permeability (mD)	Weight (g)	Length (cm)	Diameter (cm)	Total volume (cm <sup>3</sup> )	Solid volume (cm <sup>3</sup> )	Pore volume (cm <sup>3</sup> )	Bulk density (cm <sup>3</sup> )
1	2.715	23.399	7.977	60.875	6.383	2427	29.532	22.419	6.848	2.061.323
2	2.693	21.345	92.267	23.028	2.519	2347	10.894	8.552	2.321	2.113.824
3	2.693	8.38	12.9	27.600	2.547	2387	11.396	10.249	0.937	2.421.902
4	***	***	***	34.846	3.136	23,606	***	***	***	***
5	2.69	7.774	214.667	34.559	3.212	2363	14.083	12.848	1.083	2.453.952
6	2.677	11.47	2.226.667	37.180	3.606	2378	16.022	13.888	1.799	2.320.559
7	2.683	3.666	0.0001	49.709	4.329	2385	19.333	18.525	0.705	25.712
8	***	***	***	48.611	4.716	23,626	***	***	***	***
9	2.695	12.432	3.563.333	66.585	6.150	2452	29.038	24.707	3.508	229.303
10	2.689	2.527	0.0001	91.942	7.603	2447	35.761	34.201	0.887	2.571.013
11	2.708	3.648	0.0001	62.055	5.149	2449	24.247	22.913	0.868	2.559.286
12	2.711	10.382	727	65.212	5.768	2451	27.205	24.058	2.787	2.397.059
13	2.716	11.528	976	57.442	5.167	2449	24.347	21.150	2756	2.359.305
14	2.719	7.268	0.602	65.073	5.598	2440	26.184	23.930	1876	248.522
15	***	***	***	21.456	1.794	24,076	***	***	***	***
16	***	***	***	62.684	5.100	24,120	***	***	***	***
17	2.631	0.855	0.0001	72.437	6.020	2437	28.076	27.534	0.237	2.580.033

The asterisks are NULL Value. The samples with \*\*\* were not possible obtain data Total volume, density, permeabilities, and porosity values for each sample

Permeability and porosity cross-plot analyses comprise a valuable tool in understanding the distribution and variability of these two key reservoir parameters. The plot can be divided into different zones based on the clustering of data points, corresponding to different flow units with distinct permeability and porosity values.

Our findings indicate that most of the reservoir area was characterized by low permeability and low porosity, indicating low flow potential. The highest flow potential was located in thrombolite facies where the permeability and porosity values were comparatively high (Fig. 6).

### 4.3 Geochemistry

The results are expressed as ‰ units and presented regarding the PDB standard (Table 3). The international reference standard for carbon isotopes is VPDB, which is shorthand for “Vienna Pee Dee Belemnite”.

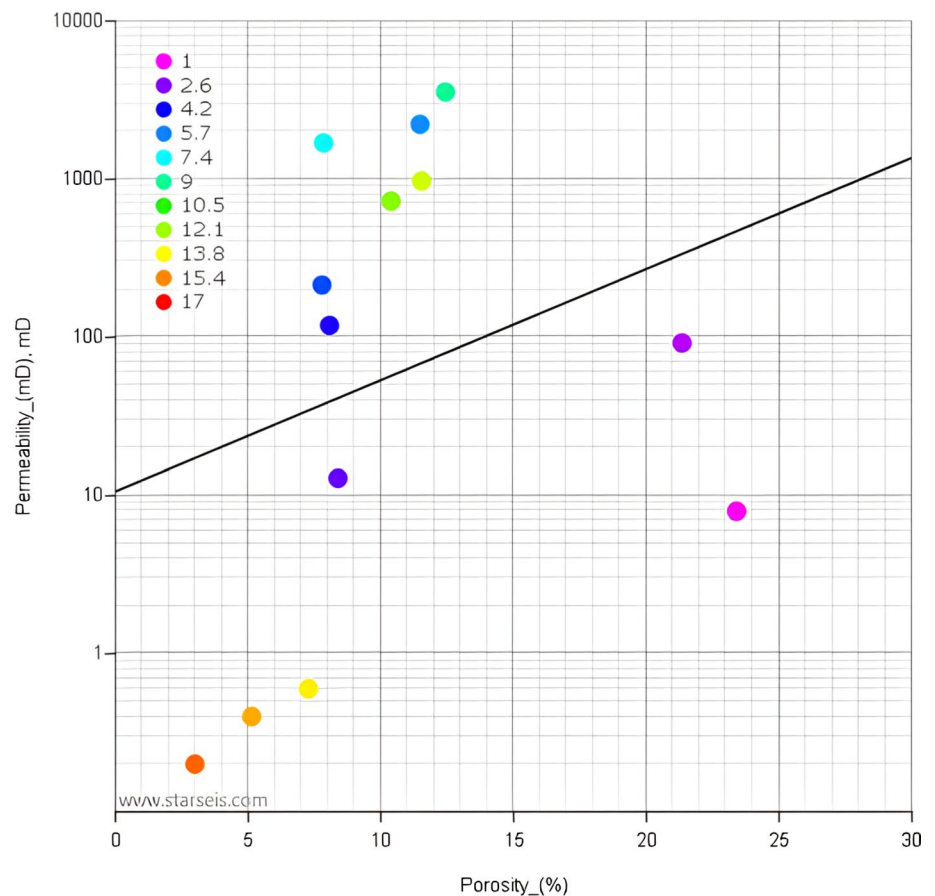
Figure 7 illustrates the integrated log-based presented permeability and porosity variation with spectral gamma ray signature and stable isotopes. The integration of the geochemical core data with the petrophysical data demonstrated that almost all measurements are consistent with the

lithologies, with no major anomalies that could falsify their interpretations, as displayed in the logs presented in Fig. 7.

Whole-rock method isotopic analyses are a method used to interpret the geochemical and isotopic signatures of rocks on a large scale using whole-rock samples., providing a broad overview of the isotopic composition of a given rock formation (Dembicki, 2017). Detailed micro-sampling from diverse depositional and diagenetic isotopic signatures, on the other hand, is a more detailed method of analyzing the isotopic composition of rocks. This method involves taking small samples from different areas of a rock formation and analyzing the isotopic signatures of these individual samples, permitting a more precise interpretation of the isotopic composition of a given rock formation (Benito et al., 2005; Melim et al., 1995).

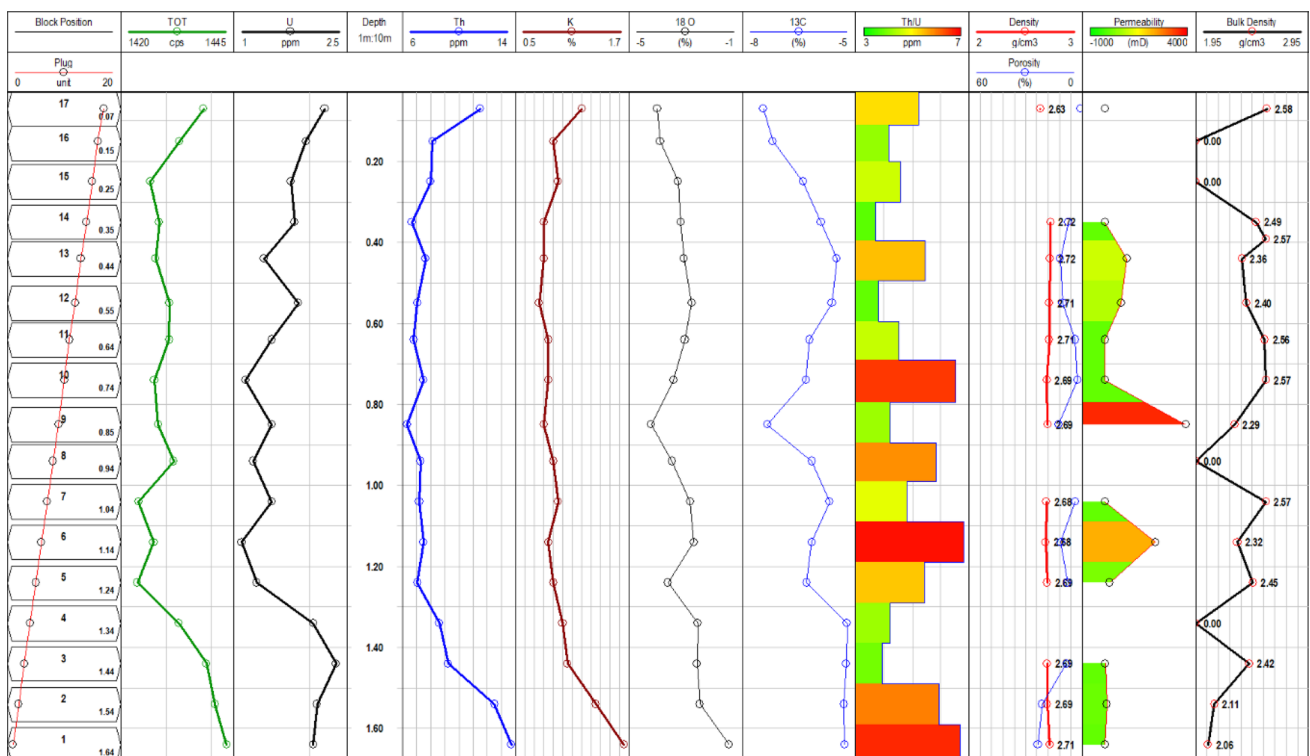
Isotopic whole-rock analyses were previously employed in a similar isotopic analysis of the same unit (Bosence & Gallois, 2022), enabling comparisons. The data indicates a similar trend for some stable isotope C and O measurements as seen in another quarry (Perryfield Quarry). Although the block used in this research is from the Bowers Quarry, similar results and a negative upwards trend were confirmed (Fig. 8).

**Fig. 6** A cross plot indicating permeability versus porosity recorded outcomes from core analysis indicates the best-fit line where heterogeneity is illustrated through the distribution interval



**Table 3** Purbeck plugs stable isotopes for  $\delta^{13}\text{C}$  (‰) VPDB e o  $\delta^{18}\text{O}$  (‰) VPDB

Plug	$\delta^{13}\text{C}$ (‰) VPDB	STD DEV	$\delta^{18}\text{O}$ (‰) VPDB	STD DEV	$\text{CO}_2$ TOTAL $\mu\text{mol mol}^{-1}$
1	-5.285	0.032	-1.452	0.067	1390
2	-5.31	0.007	-2.485	0.029	1411
3	-5.245	0.033	-2.59	0.071	1408
4	-5.225	0.019	-2.568	0.006	1314
5	-6.294	0.006	-3.629	0.01	1200
6	-6.165	0.016	-2.706	0.057	1326
7	-5.688	0.008	-2.835	0.043	1077
8	-6.164	0.024	-3.475	0.059	1349
9	-7.338	0.027	-4.217	0.066	1378
10	-6.307	0.011	-3.417	0.032	1332
11	-6.217	0.042	-3.026	0.059	1402
12	-5.619	0.035	-2.774	0.052	1317
13	-5.496	0.023	-3.056	0.038	1332
14	-5.914	0.031	-3.163	0.032	1390
15	-6.382	0.015	-3.264	0.043	1361
16	-7.196	0.012	-3.899	0.067	1346
17	-7.436	0.017	-4.000	0.05	1270

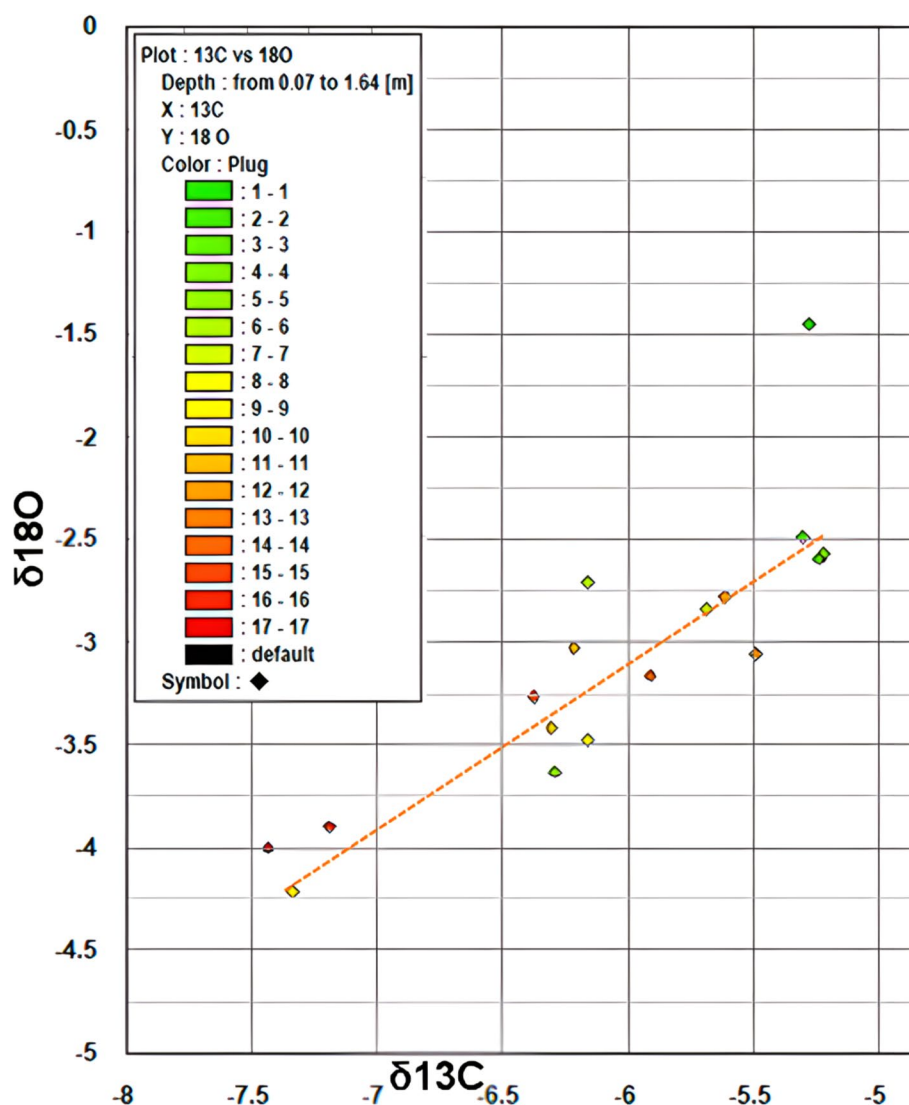
**Fig. 7** Composite log from the Hard Cap block thrombolite integrating the gamma-ray spectrometry results with selected petrophysical logs and carbon and oxygen stable isotope analyses. The plug num-

bers indicate the position of the cored intervals. This integration allows for the identification and characterization of the main Hard Cap facies

As the samples used for isotopic analyses were obtained using the whole-rock method, they represent only an average isotopic signature of all the components in each sample.

Microbialites are characteristically heterogeneous, and their components are highly diverse (*e.g.*, different types of primary micrites, bioclasts and other particles, plus different

**Fig. 8** Stable isotopes  $\delta^{13}\text{C}$  (‰) and  $\delta^{18}\text{O}$  VPDB cross-plots



types of cement precipitated at different diagenetic stages, see petrographic descriptions in the next section). All these components display different isotopic signatures; therefore, whole-rock isotopic data would only represent their average. Further detailed micro-sampling would be necessary to clearly differentiate diverse depositional and diagenetic isotopic signatures.

#### 4.4 Thin section petrography

Thin sections were observed under a microscope, photographed, and described. Four major sedimentary facies were distinguished, following the previous characterization reported by Gallois et al. (2018). The Hard Cap sedimentary facies were classified into three types: wackestone to fine grainstone facies, microbialite facies, and inter-mound facies. The microbialite facies was further divided into Thrombolite and boundstone facies, while the

inter-mound facies were composed of intraclastic peloidal packstone-grainstone.

Table 4 presents the petrographic characterization of the Hard Cap facies. The descriptions are based on the petrographic study of thin sections and consulting the previous petrographic analysis of Gallois et al. (2018), as well as the literature related to carbonate petrography (Choquette & Pray, 1970; Dunham, 1962; Folk, 1959). The porosity results were obtained from direct pore counts based on grain individualization, resulting in 2D dimensions.

Overall, the petrographic microscopy of Hard Cap Mupe Member, and lower Purbeck limestone reveals a complex and dynamic environment with frequent changes in water depth and salinity, shaped by the interplay of sedimentation and biological activity. The Hard Cap sample's main constituents are oolites, formed by physical and chemical accretion around a nucleus. Peloids and pellets are also present, comprising rounded micritic grains of various origins,

**Table 4** Petrographic analysis of thin slices from Hard Cap Purbeck plugs

Core	Petrographic Texture	Structure, texture, mineralogy and fossils	Porosity	
1	Mudstone	Dense, mottled (and locally micropeloidal) micrite, with scattered peloids and calcite pseudomorphs after gypsum. Locally, chalcedony spherulites replace the micrite	Total	~ 16%
			Matrix dissolution	8.00%
			Moldic (MO)	2.00%
			Interparticle (BP)	1.80%
			Fenestral (FE)	4.00%
2	Mudstone-Wackestone	Composed of peloids and carbonate intraclasts within a micritic matrix presenting a dense and clotted texture. Large, elongated pores with rounded sections (moulds of vegetable remains?). Chalcedony spherulites replacing the matrix. Macrocrystalline calcite fills the porosity and replaces the matrix	Total	~ 12%
			Moldic (MO)	5.00%
			Matrix dissolution	2.60%
			Interparticle (BP)	2.00%
			Intraparticle (WP)	2.00%
3	Peloidal-intraclastic grainstone	Peloids and intraclasts containing local bioclasts (ostracods). Macrocrystalline calcite cement fills interparticle spaces. Intraclasts include chalcedony spherulites replacing the micrite	Total	~ 7%
			Moldic (MO)	3.00%
			Matrix dissolution	1.70%
			Interparticle (BP)	1.00%
			Fracture (FR)	1.00%
4	Microbialite and Peloid grainstone	Partially microbialite with dense and clotted micrite microfabrics and partially peloidal and intraclastic grainstone. Macrocrystalline calcite filling porosity. Within the microbialite, one large pore with geopetal infill of peloids, intraclasts and crystalline silt	Total	~ 5%
			Moldic (MO)	3.00%
			Interparticle (BP)	1.50%
			Fracture (FR)	1.00%
5	Microbialite (thrombolite)	Microbialite irregularly shaped, dense and clotted micritic textures. Abundant chalcedony spherulites replace micrite. Large irregular pores within and around the microbialite, partially filled by peloids, intraclasts and calcite cement	Total	~ 12%
			Moldic (MO)	5.00%
			Interparticle (BP)	4.00%
			Vug (VUG)	2.00%
6	Microbialite (thrombolite)	Microbialite with irregularly shaped and dense and clotted micritic textures (thrombolite). Abundant chalcedony spherulites replace the micrite. Large irregular pores within and around the microbialite, partially filled by peloids, intraclasts and different types of cement	Total	~ 6%
			Vug (VUG)	3.00%
			Moldic (MO)	2.50%
			Interparticle (BP)	1.00%
7	Microbialite (thrombolite)	Microbialite with irregularly shaped and dense and clotted micritic textures ( <i>i.e.</i> , thrombolite). Abundant chalcedony spherulites replace micrite. Large irregular pores within and around the microbialite, partially filled by peloids, intraclasts and calcite cement	Total	~ 4%
			Interparticle (BP)	2.00%
			Moldic (MO)	1.50%
8	Microbialite (thrombolite)	Microbialite with irregularly shaped, dense, and clotted micritic textures ( <i>i.e.</i> , thrombolite). Abundant chalcedony spherulites replace the micrite. Large irregular pores within and around the microbialite, partially filled by peloids, intraclasts and calcite cement. Slight differences between the previous (microbialite) samples regarding the amount of spherulites and ostracods and pore type and infill	Total	~ 5%
			Moldic (MO)	3.00%
			Interparticle (BP)	1.00%
			Intercrystalline (BC)	1.00%
9	Microbialite (thrombolite)	Microbialite with irregularly shaped and dense and clotted micritic textures ( <i>i.e.</i> , thrombolite). Abundant chalcedony spherulites replace the micrite. Large irregular pores within and around the microbialite, partially filled by peloids, intraclasts and calcite cement	Total	11.20%
			Vug (VUG)	5.00%
			Moldic (MO)	2.00%
			Fracture (FR)	2.00%
			Intercrystalline (BC)	1.20%
10	Microbialite (thrombolite)	Microbialite with irregularly shaped and dense and clotted micritic textures ( <i>i.e.</i> , thrombolite). Abundant chalcedony spherulites replace the micrite. Large irregular pores within and around the microbialite, partially filled by peloids, intraclasts and calcite cement. Major occurrence of ostracodes, with gastropods also found	Total	~ 8.5%
			Intercrystalline (BC)	3.10%
			Moldic (MO)	2.00%
			Vug (VUG)	2.00%
			Interparticle (BP)	1.40%

**Table 4** (continued)

Core	Petrographic Texture	Structure, texture, mineralogy and fossils	Porosity	
11	Microbialite and Peloid grainstone	Partially microbialite with dense and clotted micrite microfabrics and partially, peloidal and intraclastic grainstone composed of peloids, carbonate intraclasts and bivalve and gastropod bioclasts. Porosity is reduced by cementation	Total	6.30%
			Intercrystalline (BC)	2.30%
			Moldic (MO)	2.00%
			Interparticle (BP)	1.50%
			Vug (VUG)	0.50%
12	Peloidal-intraclastic Grainstone	Peloids, intraclasts, and minor bioclasts (ostracods and gastropods). Intraclasts are microbialite fragments. Cementation by macrocrystalline calcite. Porosity partially filled by cement	Total	6.50%
			Vug (VUG)	2.50%
			Moldic (MO)	2.00%
			Interparticle (BP)	2.00%
13	Peloidal-intraclastic Grainstone	Peloids, intraclasts, and minor bioclasts (ostracods and gastropods). Intraclasts are microbialite fragments. Cementation by macrocrystalline calcite. Porosity partially filled by cement	Total	8.50%
			Moldic (MO)	3.00%
			Interparticle (BP)	2.00%
			Vug (VUG)	3.50%
14	Microbialite and Peloid grainstone	Partially microbialite with dense and clotted micrite microfabrics and partially, peloidal and intraclastic grainstone. Macrocrystalline calcite filling porosity. A laminated sedimentary accretion structure (filament structures within microbialite) is noted	Total	10.50%
			Moldic (MO)	3.00%
			Vug (VUG)	5.00%
			Interparticle (BP)	2.50%
15	Microbialite and Peloid grainstone	Microbialite with many pores filled by peloidal-intraclastic grainstone and by later cement	Total	9.20%
			Vug (VUG)	4.00%
			Interparticle (BP)	3.00%
			Moldic (MO)	2.20%
16	Peloidal-intraclastic Grainstone	Peloids, intraclasts and minor bioclasts (ostracods and gastropods). Intraclasts are fragments of microbialites. Barite cement filling locally occluding porosity	Total	10.50%
			Vug (VUG)	4.00%
			Moldic (MO)	3.50%
			Interparticle (BP)	3.00%
17	Packstone	Bioclasts (ostracods, mostly disarticulated), peloids and intraclasts. Macrocrystalline calcite cement fills porosity	Total	8.50%
			Moldic (MO)	3.00%
			Interparticle (BP)	2.00%
			Vug (VUG)	2.00%
			Intraparticle (WP)	1.50%

including fecal matter. Spherulites, particles of spherical or sub-spherical smooth or lobed edges of size typically less than 2 mm (Fig. 9A, B), are also present. Intraclasts are penecontemporaneous fragments of microbialites, which are partially lithified, eroded, and redeposited as new sediment. Bioclasts, which are the main constituents of the Hard Cap Samples, include all calcareous organisms or fragments of these structures. The matrix is also an important constituent of the and is defined as any carbonate material less than 0.0625 mm, corresponding to silt size. Cement is the infill by new mineral material of some pore space existing in the rock (Fig. 9D).

The petrographic thin sections indicate a porosity range of 4% to 16%, which can be attributed to various mechanisms, including primary depositional, secondary dissolution, and fracturing. Primary porosity is present in the form of interparticle, intraparticle, and moldic porosity, resulting

from variations in sedimentation and bioturbation during deposition. Secondary porosity can result from diagenetic processes, such as dissolution and leaching of the limestone through the action of groundwaters, which leaves channels and vugs inside the rock. The fractures (Fig. 9H) that run through the limestone layer contributed to the enhancement of primary and secondary porosity.

Ostracods (Fig. 9E) and gastropods (Fig. 9F) are also observed in the petrographic microscopy analysis. These organisms played an important role in the Hard Cap. Ostracod palaeoecology has also been used to reconstruct the environmental conditions of the Purbeck Limestone Group (Horne, 2009). Studies have verified that ostracods in the Purbeck Limestone Group were adapted to a wide range of environmental conditions, including salinity, temperature, and oxygen availability (Milner & Batten, 2002). This suggests that the Purbeck Limestone Group was a highly

dynamic environment, with frequent water depth and salinity changes.

Sample number 10 contains a significant occurrence of ostracodes and gastropods. By analyzing the distribution of ostracod assemblages in the Purbeck Group, paleontologists (Bate and Robinson 1990; Holmes, 2003; Horne, 2009; Horne et al., 2002) have inferred that the lake was shallow, warm, and restricted, with fluctuating salinity and oxygen levels due to periodic evaporation and a freshwater influx.

Calcite and silica cement (Fig. 9C) and replacement are quite common. Recent studies have investigated the relationship between different cement types and their impact on the porous characteristics of Hard Cap, Mupe Member Purbeck limestone. For example, a study conducted by Bosence and Gallois (2022) found that the presence of cement can reduce porosity. Understanding the impact of different types of cement on the porosity of limestone is essential for predicting the behavior of geological formations. Calcite is the most common cement type found in this petrographic analysis of thin slices from Hard Cap Purbeck plugs, and is formed through the precipitation of calcium carbonate. Figure 9D illustrates geopetal sediment, and Fig. 9E shows later barite crystals (red arrow) infilling framework pores.

The formation of the thrombolites present the Hard Cap, Mupe Member Lowe Purbeck Limestone is believed to have taken place in several phases. The first phase involved the colonization of the lake floor by cyanobacteria, which began to form small, spherical thrombolites. Over time, these thrombolites grew in size and complexity, eventually forming columnar structures that are present in the limestone today. A second phase of thrombolite formation occurred when the lake level rose, leading to the previously formed thrombolites being covered by sediment. As the sediment settled, it trapped pockets of lake water, allowing for the continued growth and development of the thrombolites. Finally, a third phase of thrombolite formation occurred when the lake level fell, exposing the previously buried thrombolites to the air. This exposure caused the thrombolites to dry out and become cemented together, forming the massive thrombolitic layers characteristic of the Hard Cap, Mupe Member Lowe Purbeck Limestone.

#### 4.5 X-ray microtomography (microCT)

The microCT data were recorded as object projections at different angles on a flat detector, obtaining radiographs. These radiographs then underwent a reconstruction process to generate two-dimensional tomograms (slices), which, when stacked, generate a three-dimensional image of the imaged object. The possibility of non-destructive three-dimensional visualization of the interior of rocks and automated quantitative analyses in hundreds of microtomographic sections and the volume are the main

contributions X-ray microtomography provides to petrographic and microstructural studies.

Table 5 summarizes the quantitative microtomography results, listing total porosity values obtained directly through microCT. Plugs presenting porosity over 3.00% were considered for permeability measurements, except for Plug 17, which was used as a reference to indicate that permeability in samples presenting less than 3% porosity is insignificant.

The X-ray microtomography analysis of thrombolites from the Hard Cap has provided insights into the internal structure and composition of these structures. The presence of voids and channels within the thrombolites suggests that microbial degradation plays an important role in porosity formation. The X-ray microtomography analysis revealed a complex microstructure consisting a variety of micro-features, such as pore networks, fractures, and equant grains with different mineral compositions.

The high-resolution microtomography image analysis of 3D volumes for the visualization of the three-dimensional distribution of pores, fractures, and mineralization within selected samples and facies. Their distribution is linked to facies features.

Four facies' types (A—wackestone to fine grainstone facies, B—microbialite facies, divided into Thrombolite and boundstone facies, C—inter-mound facies composed of intraclastic peloidal packstone-grainstone, and D—Packstone) were defined (Fig. 10) based in the integration of petrographic textural aspects (Table 4) with petrophysical data.

Figure 10 combines different scales of analysis, providing a comprehensive understanding of the Hard Cap samples. These included traditional macroscopic observations from the outcrop block and plugs and a microscopic petrographic examination of thin sections. From left to right: column 1 shows microscopic level petrography (optical microscopy), column 2 shows macroscopic observations from outcrop plugs; columns 3–4 show X-ray microtomography to examine the pore structure.

The pore network was verified as complex, with various pore sizes and shapes. Additionally, the connectivity of the pore network was found to vary across the formation, with some areas exhibiting high connectivity while others had low connectivity.

The facies Mudstone-Wackestone (A) have many small pores with low connectivity. The microbial facies (B) exhibit generally low primary porosity. On the other hand, calcite precipitation and its resistance to compaction influence porosity, preserving the native pore system during the burial history. In the intraclastic peloidal facies (C), the pore network was dominated by small pores with medium connectivity, which could limit the potential flow due to different types of cement. In the packstone facies (D), secondary mineralization and cement play an important role in controlling

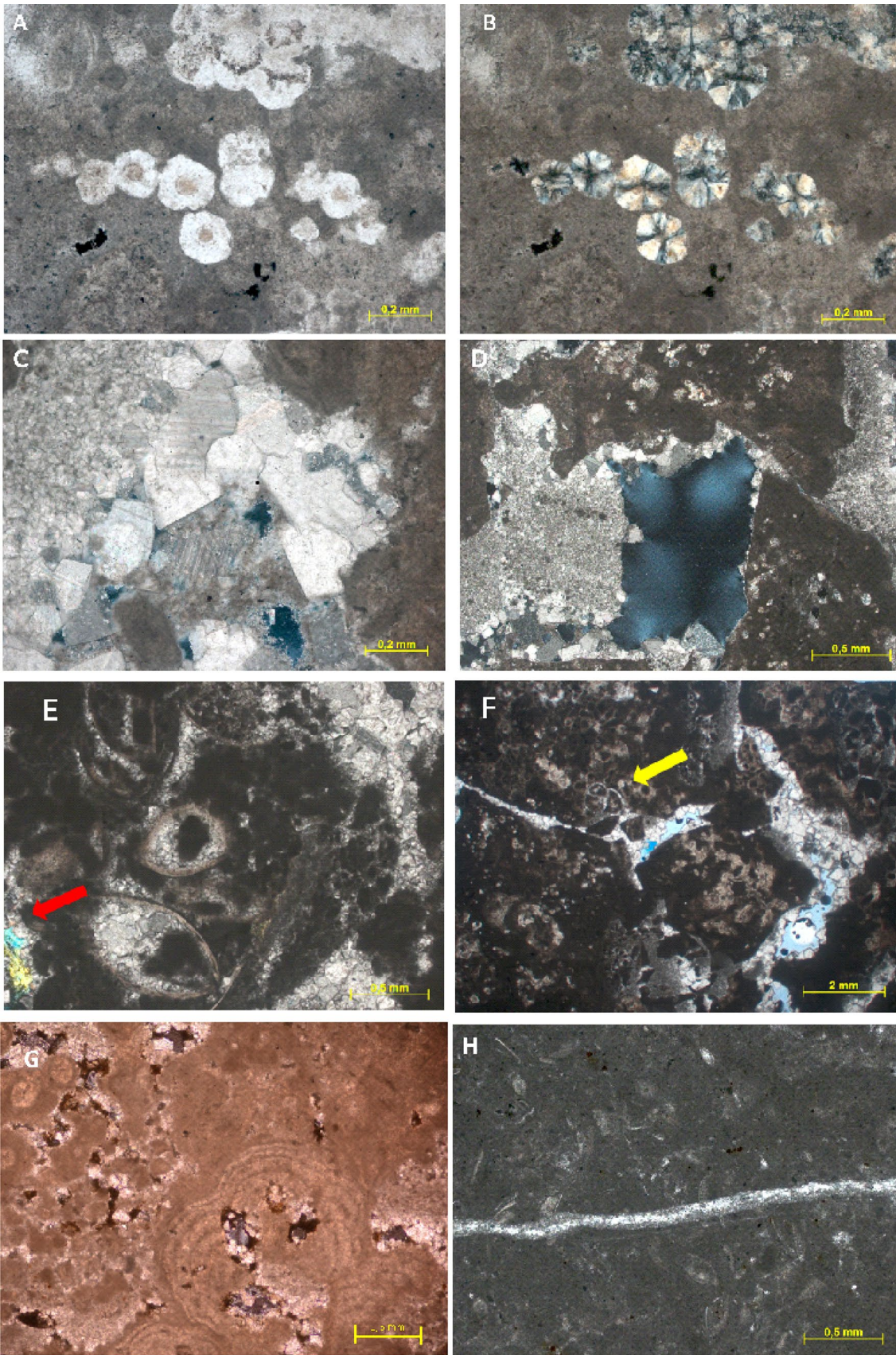




**Fig. 9** **A** Chalcedony spherulites replacing the thrombolite framework. **B** Similar view as in **A** but in cross-polarized light (XPL) illustrating radial extinction cross under polarized light—Plug 4. **C** Pores within and around the microbialite filled by different types of cement. **D** Macropore between spherulitic mesoclots partially occluded with geopetal fills in cross-polarized light (XPL)—Plug 6. **E** Peloids, intraclasts and minor bioclasts (ostracodes), barite cement filling locally occluding porosity (red arrow)—Plug 16. **F** Bioclasts (ostracods and gastropods) in cross-polarized light (XPL)—Plug 10. **G** laminated sedimentary accretion structure (filament structures within microbialite)—Plug 14. **H** Bioclasts (ostracods, mostly disarticulated), peloids and intraclasts. Calcite cement fills a fracture in Plug 17—Packstone

the rock's porosity. Small and isolated pores with low connectivity dominate the pore network.

The X-ray microtomography images were used to perform numerical simulations of fluid flow through the samples, allowing for the direct measurement of permeability. However, due to the complex pore structures of most reservoir rocks, the accuracy of X-ray microtomography-based permeability measurements can vary depending on the choice of the simulation method.

One approach to address this issue is using the flow line representative, which was introduced by Armstrong et al. (2006). This method involves tracing a large number of randomly placed streamlines through the X-ray micro-CT image and calculating the average velocity along each streamline. From this, the permeability can be calculated using Darcy's law. The advantage of this approach is that it considers the heterogeneity of the pore structure and provides a more representative measurement of permeability.

Several studies have utilized the fluid flow simulation representative method for X-ray micro-CT -based permeability analyses. For example, Zambrano et al. (2018) investigated the impact of pore scale heterogeneity on permeability using X-ray micro-CT and found that the fluid flow simulation representative method provided more accurate measurements than traditional simulation methods. Similarly, Menke et al. (2021) performed X-ray micro-CT -based permeability analyses of shale samples and found that the flow line representative method provided more accurate measurements than other simulation methods.

The 3D models of the analyzed volume depicted in Figs. 11, 12, 13, and 14 highlight the porosity present in the pore space in blue. In contrast, for permeability, the pore space is represented in red, while the flow lines in blue depict the flow simulation for permeability calculation.

Overall, X-ray microtomography was proven a valuable tool for characterizing the Hard Cap, Mupe Member, and Lower Purbeck Group. By providing high-resolution 3D imaging of the internal structure of these formations, X-ray microtomography can provide critical information for assessing their potential for hydrocarbon accumulation.

Rodrigues (2005) documented changes in the stable carbon and oxygen isotope values in the Aptian of the Campos

Basin, where the noted enrichment in the  $\delta^{18}\text{O}$  content indicated an increase in system evaporation. Bosence and Gallois (2022) provide additional evidence of lake water chemistry, showing that these trends are similar to those described for carbonates, albeit marine, below current Caribbean exposure surfaces. These modern examples indicate a 2 to 4 ‰ decrease at  $\delta^{13}\text{C}$  values and an increase of about 1 ‰ in  $\delta^{18}\text{O}$  values a few meters above the ground. The negative  $\delta^{13}\text{C}$  values are interpreted as due to  $^{12}\text{C}$  soil gas enrichment and the more positive  $\delta^{18}\text{O}$  values are due to preferential  $^{16}\text{O}$  evaporation into the soil. The similarity between these trends and those below the Purbeck karst surfaces and soil horizons is, therefore, considered to reflect early vadose diagenesis.

The integration of microtomography, petrographic, geochemistry, and petrophysics data from the Purbeck samples supports not only the identification of alterations in facies interpretation but also verifies that almost all measurements are consistent with their described lithologies. This enables inferences regarding the depositional conditions that affected the carbonate facies variations and in the recognition of the depositional cycle depicted in Fig. 15.

The porosity results obtained from thin section descriptions were integrated with laboratory petrophysics analyses, including porosimeter and microCT data. It is important to note that thin-section porosity estimates are based on direct pore counting and are limited to 2D dimensions. The log depicted in Fig. 16 summarizes the quantitative results obtained.

**Table 5** Summary of the permeability and porosity variation values determined by the microCT analyses in the studied plugs

Plug	Total volume (cm <sup>3</sup> )	Pore volume (cm <sup>3</sup> )	Total porosity (%)	Permeability (mD)
1	17.384	0.683	3.95	2.15
2	8.605	0.634	7.37	84.50
3	8.706	0.123	1.41	–
4	10.763	0.218	2.03	–
5	10.850	0.641	5.91	202.96
6	12.183	1.122	9.21	2011.63
7	14.979	0.187	1.25	–
8	11.966	0.896	7.49	2130.27
9	20.006	2.050	10.25	2336.50
10	26.742	0.544	2.03	–
11	17.760	0.155	0.87	–
12	20.005	0.749	3.74	663.91
13	18.340	0.829	4.52	467.12
14	19.499	0.141	0.72	–
15	4.795	0.004	0.07	–
16	17.695	0.018	0.1	–
17	21.165	0.003	0.02	–

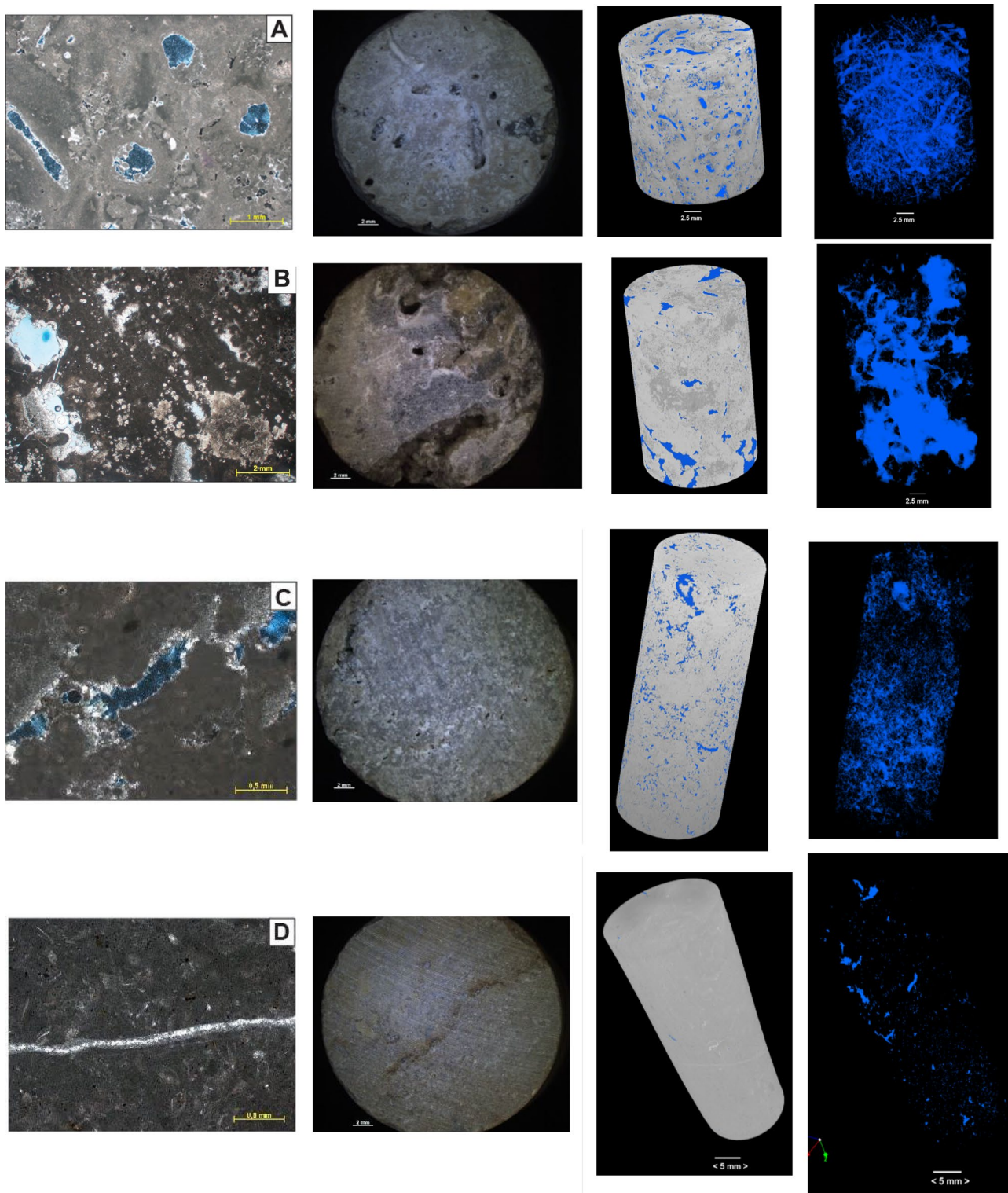


**Fig. 10** Multi-scale characterization from left to right: column 1—the microscopic level petrography (optical microscopy), column 2—macroscopic observations from outcrop plugs; column 3–4 X-ray microtomography to examine the pore structure. **A** Wackestone to

fine grainstone facies. **B** Microbialite facies, divided into Thrombolite and boundstone facies. **C** Inter-mound facies composed of intraclastic peloidal packstone-grainstone and **D** packstone

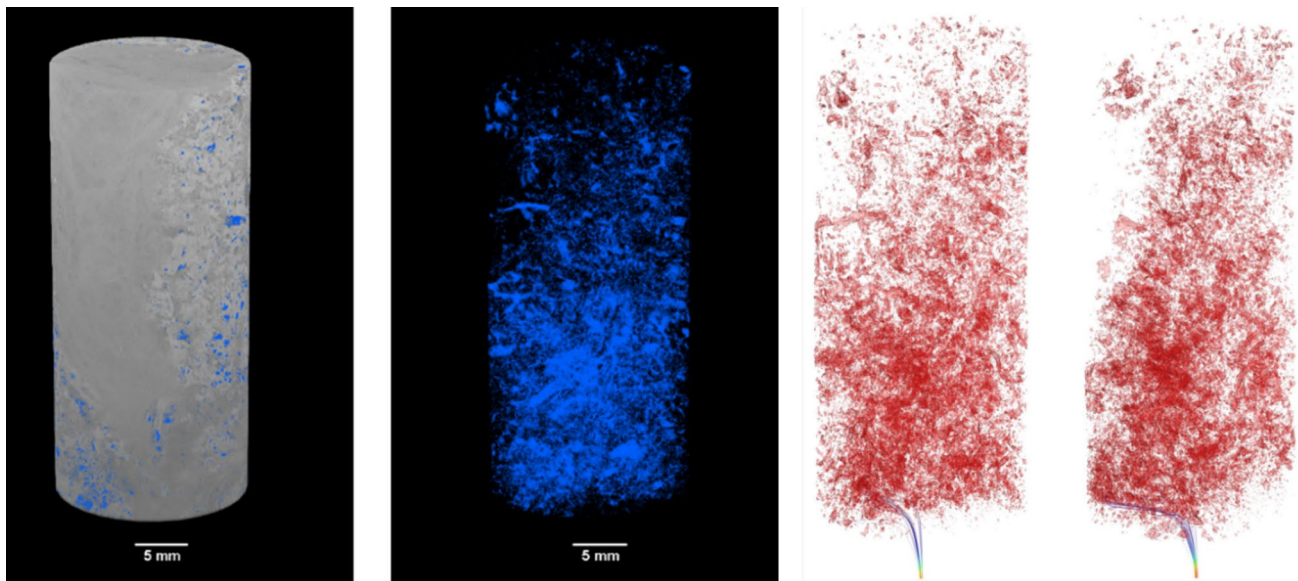


**Fig. 11** On the left, the 3D structure of the rock pore arrangement of Plug 1 (Mudstone) is in blue; on the right, the 3-D representation of porosity (in red) is generated by a microCT scan, with flow lines represented in blue

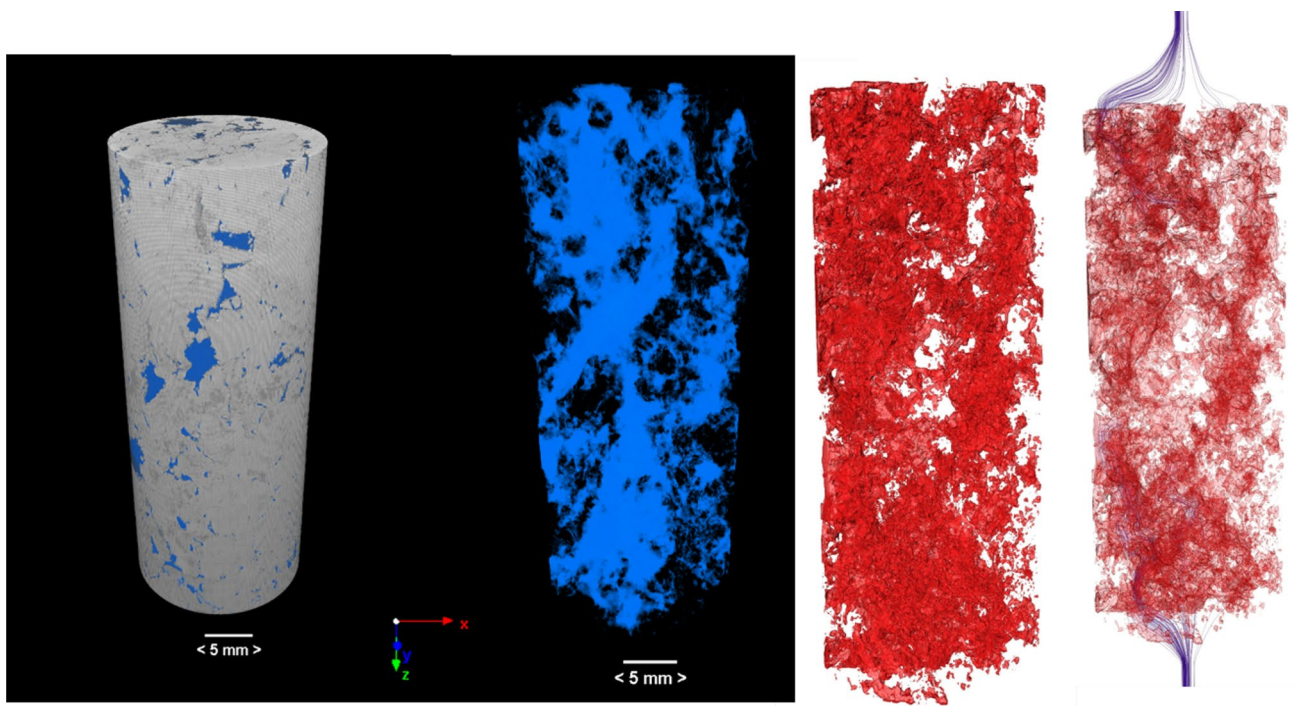


**Fig. 12** On the left, the 3D structure of the rock pore arrangement of Plug 9 Microbialite (thrombolite) in blue and on the right, the 3-D representation of porosity (in red) generated by a microCT scan, with flow lines represented in blue

Furthermore, the microCT image results were consistent with the thin-section classifications of rock texture quality. The discrepancy between porosity values can be explained by the fact that the porosity obtained by microCT consists of total porosity, which is limited by the effective pixel size

used during data acquisition. This, in turn, is associated with the sample size being investigated. Thus, pores smaller than the employed spatial resolution were not accounted for. At this point, it is important to clarify that effective pixel size is determined by the object's magnification, enabling

**Fig. 13** The 3D structure of the rock pore arrangement of Plug 16 Peloidal-intraclasts Grainstone), in blue). Local filling by a high-density material, occluding porosity. The integration of the microCT and petrographic data indicates barite

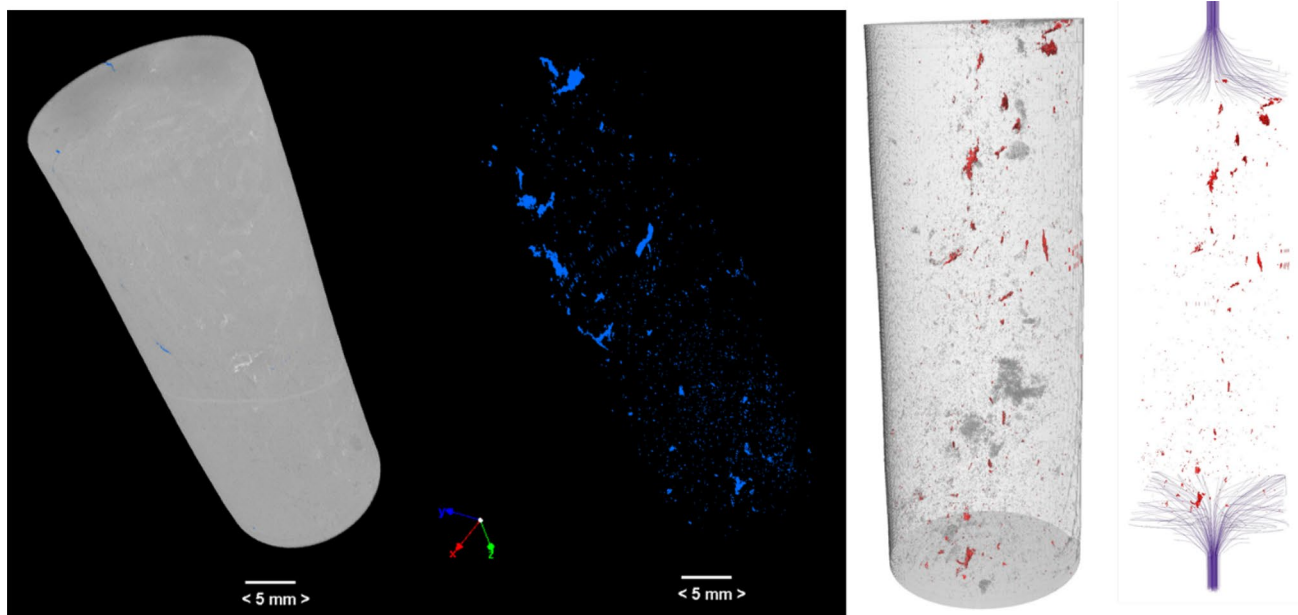
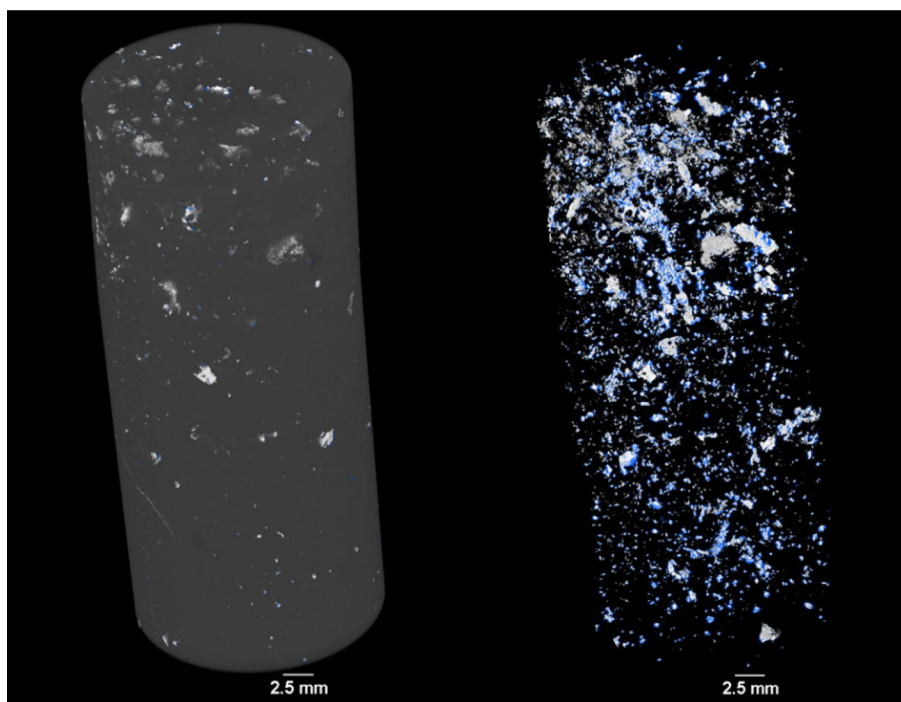


**Fig. 14** 3D analysis of sample 17's (Packstone) tomography images. The rock pore arrangement is highlighted in blue. The right-hand image depicts a 3-D representation of porosity generated and deter-

mined by a microCT scan, with permeability indicated in red, where macrocrystalline calcite cement fills any porosity. No pore connection/permeability is observed

the recognizability of the detail detectability in the image. However, the spatial resolution of the image, in addition to effective pixel size, also depends on the microCT system, penumbra blurring due to the focal spot size, X-ray source, scan conditions, and reconstruction (Rueckel et al., 2014; Singhal et al., 2013).

Notably, the thin sections were evaluated in two dimensions, while the microCT—analyzed samples were assessed in 3D. Additionally, the porosity data obtained from the porosimeter are based on Boyle's Law. During the process, nitrogen gas is released by the cylinder filling the line and

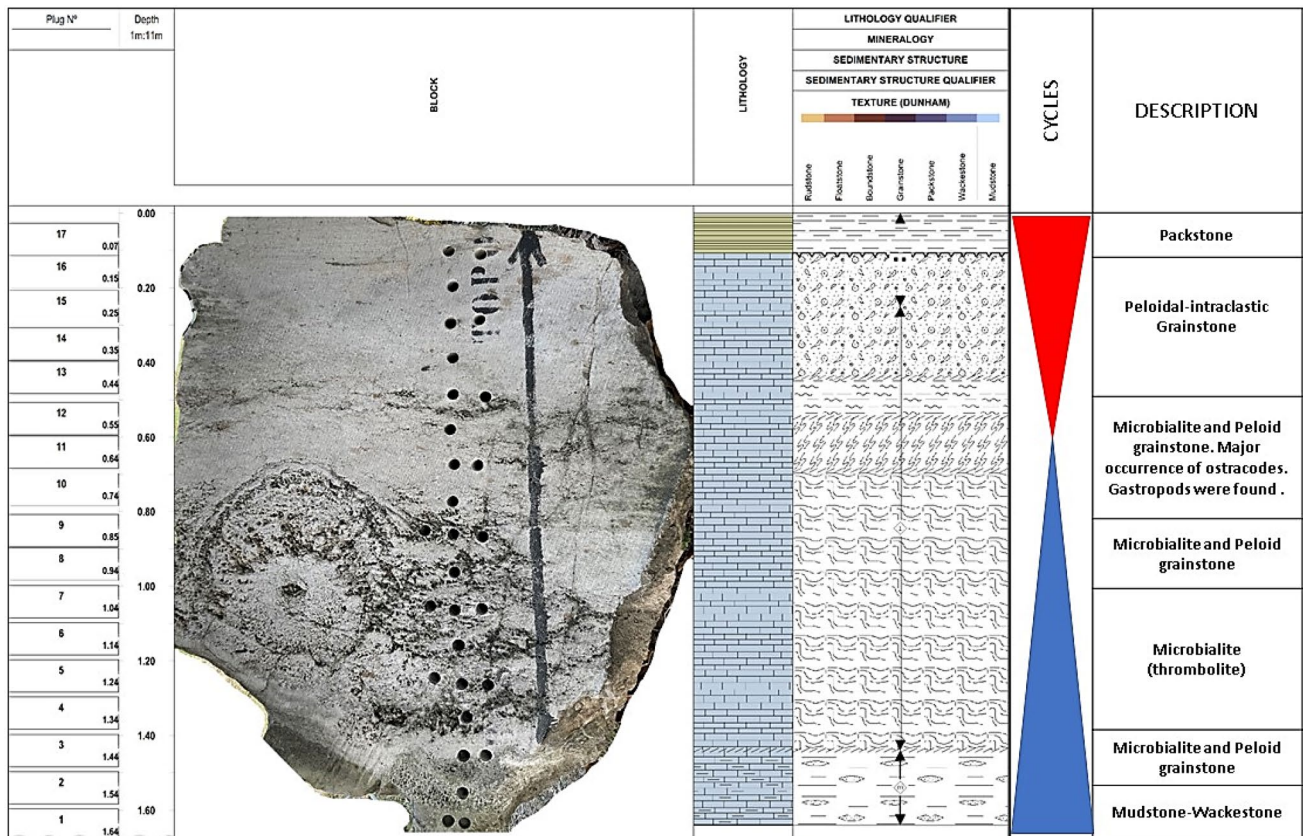


**Fig. 15** Generalized log of the Hard Cap Block. Integrating microtomography, petrographic, geochemistry and petrophysics data, it is possible to recognize the depositional cycle, detecting temporal transgressive–regressive and oxidant-reducing conditions

the internal chamber of the equipment, and the gas pressure decline is proportional to the porous volume ( $V_p$ ).

The aspect ratios of the porosity distribution from the three techniques show the same trend. These properties are affected by the diagenesis stage, which directly affects pore shape and density. The Hard Cap porosity may be either primary, generated during Microbial formation or at the end of sediment deposition, or secondary, originated by any process after rock formation or sediment deposition, such as dissolution and tectonic processes. The different types of cement and stages fill the pores, affecting permeability.

The results of this study revealed a variety of micro-structural features, including pore networks, fractures, and equant grains. The thrombolite facies were formed in shallow-water environments, characterized by warm temperatures, high evaporation rates, and low oxygen concentrations, which provided favorable conditions for microbial growth and mineral precipitation. The laboratory experiments demonstrated that the permeability and porosity of the sedimentary layers are influenced by the depositional environment, structure, and composition of the rocks, and diagenetic processes.

## 5 Conclusion

Combining different scales of analysis, a comprehensive understanding of the Hard Cap was obtained, where sedimentary cycles presenting centimetric thickness could be recognized, detecting transgressive–regressive and oxidant-reducing conditions.

The study concluded that bioturbation and dissolution are the primary factors contributing to porosity in the Hard Cap. The activity of organisms like ostracods and gastropods mixed sediment and created pore spaces, leading to increased porosity. Additionally, the dissolution of carbonate minerals also contributed to the development of porosity, with greater dissolution occurring during periods of increased groundwater flow.

Stable isotope analysis suggested that the dissolution in the Hard Cap was likely caused by acidic groundwater, which dissolved the carbonate minerals in the limestone. The isotopic analysis using the whole-rock method showed a similar negative upwards trend in previous studies. However, detailed micro-sampling would be necessary to distinguish between various depositional and diagenetic isotopic signatures.

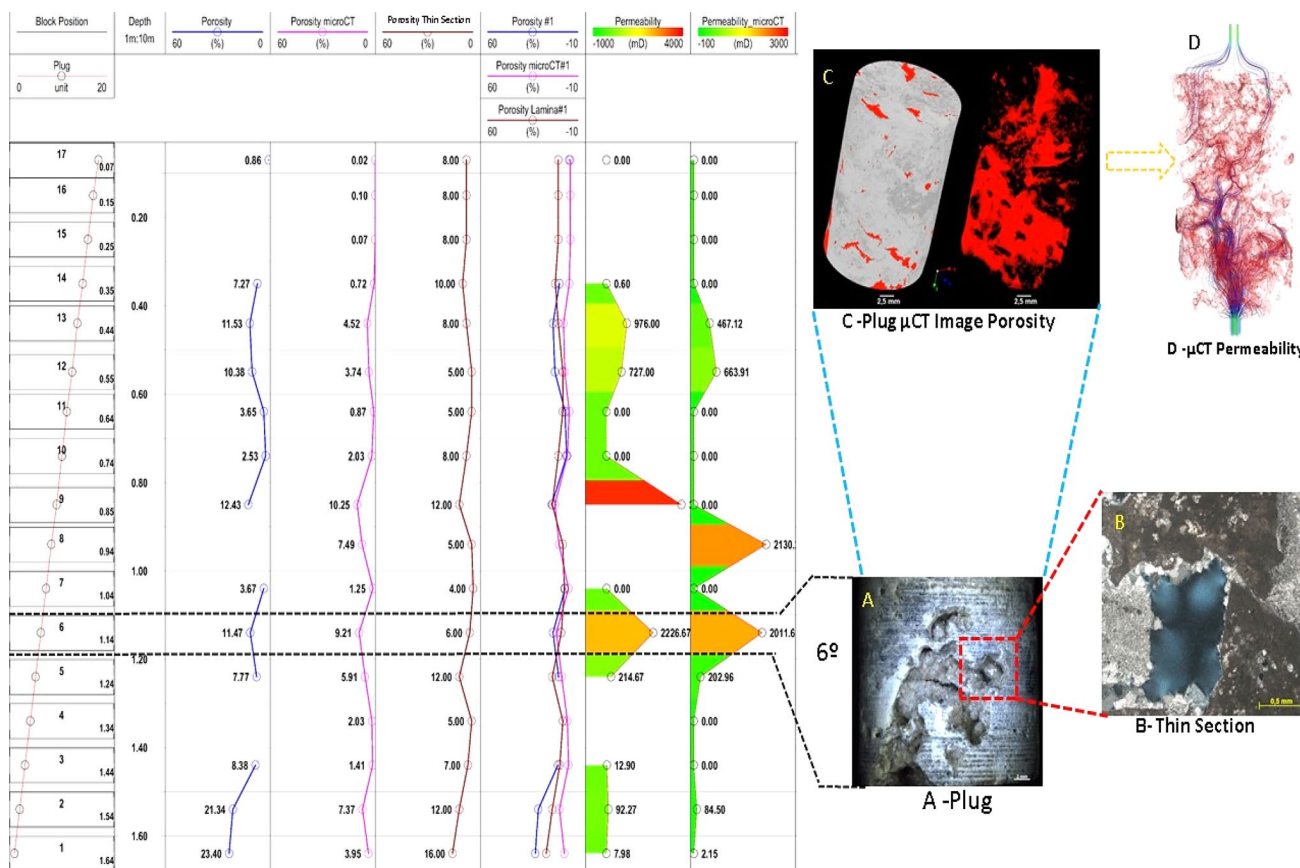


**Fig. 16** The integration log for porosity and permeability from microtomography, petrophysics and petrograph thin section analyses provides a multi-resolution and multi-scale methodology. **A** 3D structure of the solid matrix of plug 6. **B** Thin section macropore between spherulitic mesoclots partially occluded with geopetal fills in cross-

polarized light (XPL). **C** 3D structure of the rock pore arrangement with the solid matrix of plug 6 and pore arrangement comparison. **D** pore disposition in sample 6 with a 3-D representation of the porosity generated by the image analysis of a microCT scan, where flow lines in blue represent permeability at 50% transparency

The cementation process was identified as the primary cause of the Hard Cap's low porosity and permeability. The analysis also revealed that the Hard Cap was deposited in a shallow environment with alternating periods of subaerial exposure and inundation.

The paleo controls on porosity development in the Hard Cap were found to be largely related to changes in lake level and climate. During periods of high lake level, the Hard Cap was submerged and subject to increased sedimentation, leading to reduced porosity development. In contrast, during periods of low lake level, the Hard Cap was exposed to increased groundwater flow, which promoted dissolution and porosity development.

X-ray microtomography was proven a valuable tool for characterizing the Hard Cap, Mupe Member, and Lower Purbeck Group. By providing high-resolution 3D imaging of the internal structure of these formations, X-ray microtomography can provide critical information for assessing their potential for hydrocarbon accumulation. The estimated petrophysics matched the dominant Hard

Cap rock textures identified by microCT, establishing the relationship between physical laboratory data and pore-scale imaging analyses towards a more holistic understanding of reservoir quality. Thin-section petrographic analyses and laboratory methods provide quality control for relative microCT permeability.

Due to the high costs of taking core samples and the lack of available Brazilian pre-salt rock samples, the integrated assessment presented herein offers an excellent opportunity to understand petrophysical responses and their relationship with different facies in order to more accurately evaluate and characterize carbonates from a porosity distribution perspective.

Overall, this study provides important insights into the porosity and permeability in the Hard Cap of the Mupe Member and the controls that influenced its development. The findings of this study and the applied methodologies may be useful in the exploration and development of hydrocarbon reservoirs located in similar geological settings.

**Acknowledgements** Special thanks are due to Drs. Pablo Suarez-Gonzalez and M. Isabel Benito from the Complutense University of Madrid (Spain), for their help in the description and interpretation of petrographic and geochemical data. We also would like to thank Dr. Arnaud Gallois (Royal Holloway University of London) and Dr. Peter Burgess (University of Liverpool, UK) for their guidance and discussions during the field trip in south Dorset. We would also like to thank Bernard Vining and Professor Dan Bosence (Royal Holloway University of London) for all the guidance and support. The authors also thank Baker Hughes of Brazil for donating the blocks used in this research to the State University of Rio de Janeiro (UERJ). We would like to thank the National Observatory Petrophysics Laboratory (LabPetrON) team for performing the routine petrophysics analyses, the UERJ Chemostratigraphy and Organic Geochemistry Laboratory (LGQM-UERJ) team for conducting the geochemistry isotopic analyses, and the Federal University of Rio de Janeiro Nuclear Instrumentation laboratory (UFRJ/ COPPE/ Nuclear Engineering Program) team for carrying out the microCT imaging.

**Author contributions** RCB wrote the main manuscript text and ASM and OMOA prepared micro-CT figures. All authors reviewed the manuscript.

**Data availability** The data supporting this work are available in tables and as supplementary materials.

## Declarations

**Conflict of interest** The authors are unaware of any conflict of interest regarding this work. The authors declare that they have no known competing financial interests or personal relationships that could have appeared to influence the work reported in this paper.

**Ethical approval** The authors followed the ethical standards.

**Consent to participate** Authors have consent to participate.

**Consent to publish** Authors have consent to publish. This research has been done in collaboration with researchers at Royal Holloway University of London and University of Liverpool.

## References

- Ahr, W. (2008). *Geology of carbonate reservoirs* (p. 277). John Wiley & Sons, Inc. <https://doi.org/10.1002/9780470370650>
- Anderson, F. W. (1973). The Jurassic-Cretaceous transition: The non-marine Ostracod Faunas. In R. R. Casey & P. F. Rawson (Eds.), *The boreal lower cretaceous* (pp. 101–110). Seel House Press.
- Anderson, F. W., & Bazley, R. A. B. (1971). The Purbeck beds of the Weald (England). *Bulletin of the Geological Survey of Great Britain*, 34, 1–173.
- Armstrong, R. T., McClure, J. E., & Vogler, D. R. (2006). Measurement of rock permeability using X-ray microtomography. *Geophysical Research Letters*, 33(24), L24405. <https://doi.org/10.1029/2006GL028242>
- Bate, R. H., & Robinson, E. (1990). Ostracoda from the Purbeck Limestone Group (Upper Jurassic-Lower Cretaceous) of Dorset, southern England. *Bulletin of the British Museum (natural History) Geology*, 46(3), 155–253.
- Batten, D. J. (2002). Palaeoenvironmental setting of the Purbeck Limestone Group. *Special Papers in Palaeontology*, 68, 13–20.
- Benito, M. I., Lohmann, K. C., & Ramón, M. J. (2005). Late Jurassic Paleogeography and Paleoclimate in the northern Iberian Basin of Spain: Constraints from diagenetic records in reefal and continental carbonates. *Journal of Sedimentary Research*, 75(1), 82–96. <https://doi.org/10.2110/jsr.2005.008>
- Boomer, I., Horne, D., & Slipper, I. (2003). The use of ostracods in palaeoenvironmental studies, or what can you do with an ostracod shell? *The Paleontological Society Papers*, 9, 153–180. <https://doi.org/10.1017/S1089332600002199>
- Bosence, D., & Gallois, A. (2022). How do thrombolites form? Multiphase construction of lacustrine microbialites, Purbeck limestone group, (Jurassic), Dorset, UK. *Sedimentology*, 69, 914–953. <https://doi.org/10.1111/sed.12933>
- Bosence, D. W. J. (1987). Portland and Purbeck formations of the isle of Portland. In: 4th symposium on fossil algae. Excursions Guide, Cardiff
- Butler, M. B. (1998). The geological history of the southern Wessex Basin: A review of new information from oil exploration. *Geological Society, London, Special Publications*, 133, 67–86. <https://doi.org/10.1144/GSL.SP.1998.133.01.04>
- Capezzuoli, E., Della Porta, G., Rogerson, M., & Tagliasacchi, E. (2022). Non-marine carbonate: Wherefore art thou? *Depositional Rec*, 8, 4–8. <https://doi.org/10.1002/dep2.170>
- Capezzuoli, E., & Swennen, R. (2017). Non-marine carbonates: A multidisciplinary approach. *Quaternary International*. <https://doi.org/10.1016/j.quaint.2017.04.005>
- Choquette, P. W., & Pray, L. C. (1970). Geologic nomenclature and classification of porosity in sedimentary carbonates. *AAPG Bulletin*. <https://doi.org/10.1306/5d25c98b-16c1-11d7-8645000102c1865d>
- Clements, R. G. (1993). Type section of the Purbeck Limestone Group, Durlston Bay, Swanage, Dorset. In: Proceedings of the Dorset Natural History and Archaeological Society, 114 (for 1992), pp. 181–206. <https://wessexcoastgeology.soton.ac.uk/purbfac.htm>
- Cope, J. C. W., Getty, T. A., Howarth, M. K., Morton, N., Torrens, H. S. (1980). A Correlation of Jurassic Rocks in the British Isles. Part One: Introduction and Lower Jurassic. *Special Report of the Geological Society of London*, 14, 1–73.
- Cope, J. C. W., Ingham, J. K., & Rawson, P. F. (1999). Atlas of Paleogeography and Lithofacies. *Geological Society Memoir*, 137(4), 463–479. <https://doi.org/10.1017/S0016756800354413>. First published 1992; London, Bath: Geological Society of London. Geological Magazine.
- Coram, R. A., & Radley, J. D. (2021). Revisiting climate change and palaeoenvironments in the Purbeck Limestone Group (Tithonian–Berriasian) of Durlston Bay, southern UK. *Proceedings of the Geologists, Proceedings of the Geologists' Association*, 132(3), 392–404. <https://doi.org/10.1016/j.pgeola.2021.03.001>
- Davies, S. J., & Elliott, T. (1996). Spectral gamma ray characterization of high-resolution sequence stratigraphy: Examples from Upper Carboniferous fluvio-deltaic systems, County Clare, Ireland. *Geological Society, London, Special Publications*, 104(1), 25–35. <https://doi.org/10.1144/GSL.SP.1996.104.01.03>
- Dembicki, H. (2017). *Practical petroleum geochemistry for exploration and production* (2nd ed.). Elsevier. <https://doi.org/10.1016/C2014-0-03244-3>
- Dunham, R. J. (1962). Classification of carbonate rocks according to depositional texture. In W. E. Ham (Ed.), *Classification of carbonate rocks: A symposium* (pp. 108–121). Tulsa: AAPG. <https://doi.org/10.1306/M1357>
- Dypvik, H., & Eriksen, D. Ø. (1983). Natural radioactivity of clastic sediments and the contributions of U, TH and K. *Journal of Petroleum Geology*, 5(4), 409–416. <https://doi.org/10.1111/j.1747-5457.1983.tb00592.x>

- Eberli, G., Baechele, G., Anselmetti, F., & Incze, M. (2003). Factors controlling elastic properties in carbonate sediments and rocks. *The Leading Edge*, 22(7), 654–660. <https://doi.org/10.1190/1.1599691>
- Ehrenberg, S. N., & Svånå, T. A. (2001). Use of spectral gamma-ray signature to interpret stratigraphic surfaces in carbonate strata: An example from the Finnmark carbonate platform (Carboniferous–Permian) Barents Sea. *AAPG Bulletin*, 85(2), 295–308. <https://doi.org/10.1306/8626C7C1-173B-11D7-8645000102C1865D>
- Fertl, W. H., & Rieke, H. H., III. (1980). Gamma ray spectral evaluation techniques identify fractured shale reservoirs and source-rock characteristics. *Journal of Petroleum Technology*, 32(11), 2053–2062. <https://doi.org/10.2118/8454-PA>
- Flügel, E. (2010). *Microfacies of carbonate rocks. Analysis, interpretation and application* (2nd ed., p. 976). Springer-Verlag. <https://doi.org/10.1007/978-3-642-03796-2>
- Folk, R. L. (1959). Practical petrographic classification of limestones. *AAPG Bulletin*, 43(1), 1–38. <https://doi.org/10.1306/0BDA5C36-16BD-11D7-8645000102C1865D>
- Folk, R. L. (1962). Spectral subdivision of limestone types. In W. E. Ham (Ed.), *Classification of carbonate Rocks-a symposium* (1st ed., pp. 62–84). AAPG Memoir. <https://doi.org/10.1306/M1357>
- Folk, R. L. (1974). *Petrology of sedimentary rocks* (p. 182). Hemphill Publishing Co.
- Francis, J. (1982). The fossil forests of the basal Purbeck formation (upper Jurassic) of Dorset, Southern England. Palaeobotanical and paleoenvironmental investigations (PhD Thesis), University of Southampton). <http://eprints.soton.ac.uk/id/eprint/388126>
- Francis, J. (1984). The seasonal environment of the Purbeck (Upper Jurassic) fossil forests. *Palaeogeography, Palaeoclimatology, Palaeoecology*, 48, 285–307. [https://doi.org/10.1016/0031-0182\(84\)90049-X](https://doi.org/10.1016/0031-0182(84)90049-X)
- Gallois, A. (2016). Late Jurassic lacustrine carbonates: a multi-scale analysis of the Mupe Member (Purbeck limestone group) of the Wessex basin, UK. 2016. (PhD Thesis). Royal Holloway, University of London. <https://pure.royalholloway.ac.uk/en/publications/late-jurassic-lacustrine-carbonates-a-multi-scale-analysis-of-the>
- Gallois, A., & Bosence, D. (2017). Syn-rift lacustrine carbonates; cycles, microbial mounds, and brackish to hypersaline facies models; Purbeck group, Wessex Basin, UK. Analogues for South Atlantic Pre-salt carbonates? Conference on African E&P, 31st august- 1st September 2017, London UK. [https://www.researchgate.net/profile/Arnaud-Gallois/publication/319155704\\_Syn-rift\\_lacustrine\\_carbonates\\_cycles\\_microbial\\_mounds\\_and\\_brackish\\_to\\_hypersaline\\_facies\\_models\\_Purbeck\\_Group\\_Wessex\\_Basin\\_UK\\_Analogues\\_for\\_south\\_Atlantic\\_pre-salt\\_carbonates/links/599599b4a6fdccabdd40950/Syn-rift-lacustrine-carbonates-cycles-microbial-mounds-and-brackish-to-hypersaline-facies-models-Purbeck-Group-Wessex-Basin-UK-Analogues-for-south-Atlantic-pre-salt-carbonates.pdf](https://www.researchgate.net/profile/Arnaud-Gallois/publication/319155704_Syn-rift_lacustrine_carbonates_cycles_microbial_mounds_and_brackish_to_hypersaline_facies_models_Purbeck_Group_Wessex_Basin_UK_Analogues_for_south_Atlantic_pre-salt_carbonates/links/599599b4a6fdccabdd40950/Syn-rift-lacustrine-carbonates-cycles-microbial-mounds-and-brackish-to-hypersaline-facies-models-Purbeck-Group-Wessex-Basin-UK-Analogues-for-south-Atlantic-pre-salt-carbonates.pdf)
- Gallois, A., Bosence, D., & Burgess, P. M. (2018). Brackish to hypersaline facies in lacustrine carbonates: Purbeck limestone group, Upper Jurassic-Lower Cretaceous, Wessex Basin, Dorset UK. *Facies*, 64(12), 1–39. <https://doi.org/10.1007/s10347-018-0525-4>
- Hassan, M., Hossin, A., & Combaz, A. (1976). Fundamentals of the differential gamma ray log - interpretation technique. Paper presented at the SPWLA 17th Annual Logging Symposium, One-Petro, Denver, Colorado, June 1976. <https://onepetro.org/SPWLA/ALS/proceedings-pdf/SPWLA-1976/All-SPWLA-1976/SPWLA-1976-H/2057617/spwla-1976-h.pdf>
- Hawkes, P. W., Fraser, A. J., & Eincomb, C. C. G. (1998). The tectono-stratigraphic development and exploration history of the Weald and Wessex Basins, southern England, UK. In J. R. Underhill (Ed.), *The development, evolution and petroleum geology of the Wessex Basin* (133rd ed., pp. 39–66). Geological Society London Special Publications. <https://doi.org/10.1144/GSL.SP.1998.133.01.03>
- Holmes, J. (2003). Future trends and goals in ostracode research. *The Paleontological Society Papers*, 9, 275–290. <https://doi.org/10.1017/S108933260002254>
- Horne, D. J. (2009). *Purbeck–Wealden ostracods in British stratigraphy*. J. E. Whittaker, M. B. Hart. <https://doi.org/10.1144/TMS003.12>
- Horne, D. J., Cohen, A., & Martens, K. (2002). Taxonomy, morphology and biology of quaternary and living ostracoda. *Washington DC American Geophysical Union Geophysical Monograph Series*, 131, 5–36. <https://doi.org/10.1029/131GM02>
- Jones, B., & Renaut, R. W. (1995). Noncrystallographic calcite dendrites from hot-spring deposits at Lake Bogoria, Kenya. United States. <https://www.osti.gov/biblio/37117>
- Kennard, J. M., & James, N. (1986). Thrombolites and stromatolites; two distinct types of microbial structures. *Palaios*, 1(5), 492–503. <https://doi.org/10.2307/3514631>
- Kirkham, A., & Tucker, M. E. (2018). Thrombolites, spherulites and fibrous crusts (Holkerian, Purbeckian, Aptian): Context, fabrics and origins. *Sedimentary Geology*, 374, 69–84. <https://doi.org/10.1016/j.sedgeo.2018.07.002>
- Klaja, J., & Dudek, L. (2016). Geological interpretation of spectral gamma ray (SGR) logging in selected boreholes. *Nafta Gaz*, 72(1), 3–14. <https://doi.org/10.18668/NG2016.01.01>
- Lake, S.D. (1985). The structure and evolution of the Wessex Basin (PhD Thesis), Durham University. <https://ethos.bl.uk/OrderDetails.do?uin=uk.bl.ethos.356634>
- Liu, L., Dong, Z., & Cao, H. (2017). Imaging the internal microstructure of thrombolites using micro-CT scanning. *Journal of Paleontology*, 91(4), 774–785. <https://doi.org/10.1017/jpa.2017.6>
- Lucia, F. J. (1999). Carbonate reservoir characterization: An integrated approach. *Springer Science and Business Media*. <https://doi.org/10.1007/978-3-662-03985-4>
- Luczaj, J. A. (1998). Regional and stratigraphic distribution of uranium in the Lower Permian Chase Group carbonates of southwest Kansas. *The Log Analyst*, 39(04), 1998.
- McCrea, J. M. (1950). On the isotopic chemistry of carbonates and a paleotemperature scale. *The Journal of Chemical Physics*, 18(6), 849–857. <https://doi.org/10.1063/1.1747785>
- Melim, L. A., Swart, P. K., & Maliva, R. G. (1995). Meteoric-like fabrics forming in marine waters: Implications for the use of petrography to identify diagenetic environments. *Geology*, 23(8), 755–758. [https://doi.org/10.1130/0091-7613\(1995\)023%3c0755:MLFFIM%3e2.3.CO;2](https://doi.org/10.1130/0091-7613(1995)023%3c0755:MLFFIM%3e2.3.CO;2)
- Menke, H. P., Maes, J., & Geiger, S. (2021). Upscaling the porosity–permeability relationship of a microporous carbonate for Darcy-scale flow with machine learning. *Science and Reports*, 11, 2625. <https://doi.org/10.1038/s41598-021-82029-2>
- Milner, A. R., & Batten, D. J. (2002). Life and environments in Purbeck times. *Special Papers in Palaeontology*, 68, 1–268.
- Muniz, M. C., & Bosence, D. W. J. (2015). Pre-salt microbialites from the Campos Basin (offshore Brazil): Image log facies, facies model and cyclicity in lacustrine carbonates. *Geological Society, London, Special Publications*, 418(1), 221–242. <https://doi.org/10.1144/sp418.10>
- North, C. P., & Boering, M. (1999). Spectral gamma-ray logging for facies discrimination in mixed fluvial-eolian successions: A cautionary tale. *AAPG Bulletin*, 83(1), 155–169.
- Perry, E. C. (1994). Freshwater tufa stromatolites in the basal Purbeck Formation (Upper Jurassic), Isle of Portland Dorset. *Geological Journal*, 29(2), 119–135. <https://doi.org/10.1002/gj.3350290203>
- Pugh, M. E. (1968). Algae from the Lower Purbeck Limestones of Dorset. *Proceedings of the Geologists' Association*, 79(4), 513–523. [https://doi.org/10.1016/S0016-7878\(68\)80018-5](https://doi.org/10.1016/S0016-7878(68)80018-5)
- Reid, R. P. (2001). *Thrombolites: Microbially mediated sedimentary structures Part of the Encyclopedia of Earth Sciences Series book*



- series (EESS). Elsevier. [https://doi.org/10.1007/978-1-4020-9212-1\\_196](https://doi.org/10.1007/978-1-4020-9212-1_196)
- Rodrigues, R. (2005). Chemostratigraphy. In E. A. M. Koutsoukos (Ed.), *Applied stratigraphy. Topics in geobiology* (pp. 165–178). Springer. [https://doi.org/10.1007/1-4020-2763-X\\_8](https://doi.org/10.1007/1-4020-2763-X_8)
- Rueckel, J., Stockmar, M. S., Pfeuffer, F., & Herzen, J. (2014). Spatial resolution characterization of a X-ray microct system. *Applied Radiation and Isotopes*, 94, 230–234. <https://doi.org/10.1016/j.apradiso.2014.08.014>
- Scholle, P. A., & Ulmer-Scholle, D. S. (2003). *A color guide to the petrography of carbonate rocks: grains, texture, porosity and diagenesis* (77th ed., p. 459). AAPG Memoir. <https://doi.org/10.1306/M77973>
- Serra, O. (1984). 7. Natural gamma-ray spectrometry developments in petroleum science. *Elsevier*, 15, 113–134. [https://doi.org/10.1016/S0376-7361\(08\)70421-7](https://doi.org/10.1016/S0376-7361(08)70421-7)
- Singhal, A., Grande, J. C., & Zhou, Y. (2013). Micro/nano-CT for visualization of internal structures. *Microscopy Today*, 21(2), 16–22. <https://doi.org/10.1017/S1551929513000035>
- Tucker, M. E., & Wright, V. P. (1990). *Carbonate sedimentology* (p. 252). Blackwell Scientific publications. <https://doi.org/10.1002/9781444314175>
- Underhill, J. R. (2002). Evidence for structural controls on the deposition of the Late Jurassic-Early Cretaceous Purbeck limestone group, Dorset, southern England. In A. R. Milner & D. J. Batten (Eds.), *Life and environments in Purbeck times. Special Papers in Palaeontology, volume 68* (pp. 21–40). Palaeontological Association London.
- Underhill, J. R., & Stoneley, R. (1998). Introduction to the development, evolution and petroleum geology of the Wessex Basin. *Geological Society, London, Special Publications*, 133, 1–18. <https://doi.org/10.1144/GSL.SP.1998.133.01.01>
- Webster, T. (1826). Observations on the Purbeck and Portland beds. *Transactions of the Geological Society of London*, 1, 37–44. <https://doi.org/10.1144/transgslb.2.1.37>
- West, I. M. (1975). Evaporites and associated sediments of the basal Purbeck formation (Upper Jurassic) of Dorset. *Proceedings of the Geologists' Association*, 86(2), 205–225. [https://doi.org/10.1016/S0016-7878\(75\)80101-5](https://doi.org/10.1016/S0016-7878(75)80101-5)
- West, IM. (2013). Purbeck formation—facies and palaeoenvironments. Version 2. Internet webpage: <http://www.southampton.ac.uk/~imw/purbfac.htm>
- Westhead, R. K., & Mather, A. E. (1996). An updated lithostratigraphy for the Purbeck limestone group in the Dorset type-area. *Proceedings of the Geologists' Association*, 107(2), 117–128. [https://doi.org/10.1016/S0016-7878\(96\)80005-8](https://doi.org/10.1016/S0016-7878(96)80005-8)
- Wimbledon, W. A., & Hunt, C. O. (1983). The Portland-Purbeck junction (Portlandian-Berriasian) in the Weald, and correlation of atest Jurassic–early Cretaceous rocks in southern England. *Geological Magazine*, 120(3), 267–280. <https://doi.org/10.1017/S0016756800025450>
- Woodward, H.B. (1895). The middle and upper Oolitic rocks of England (Yorkshire excepted). <https://www.cambridge.org/core/journals/geological-magazine/article/iimemoirs-of-the-geological-survey-of-the-united-kingdom-the-jurassic-rocks-of-britain-vol-v-the-middle-and-upper-oolitic-rocks-of-england-yorkshire-excepted-by-horace-b-woodward-fgs-8vo-ppxiv-and-499-145-figures-and-map-london-dulau-co-1895/23651AF00A5543E12C09EBAFE6CBF959>
- Zambrano, M., Tondi, E., Mancini, L., Lanzafame, G., Trias, F.X., Arzilli, F., Materazzi, M. & Torrieri, S. (2018). Fluid flow simulation and permeability computation in deformed porous carbonate grainstones. *Advances in water resources*, 115, 95–111.
- Ziegler, P. A. (1990). *Geological Atlas of Western and Central Europe* (p. 239). Shell International Petroleum.

**Publisher's Note** Springer Nature remains neutral with regard to jurisdictional claims in published maps and institutional affiliations.

Springer Nature or its licensor (e.g. a society or other partner) holds exclusive rights to this article under a publishing agreement with the author(s) or other rightsholder(s); author self-archiving of the accepted manuscript version of this article is solely governed by the terms of such publishing agreement and applicable law.